CrossMark

ORIGINAL PAPER

Investigating the mechanisms of diurnal rainfall variability over Peninsular Malaysia using the non-hydrostatic regional climate model

Ahmad Fairudz Jamaluddin[1,2] · Fredolin Tangang[1,3] · Jing Xiang Chung[1] · Liew Juneng[1] · Hidetaka Sasaki[4] · Izuru Takayabu[4]

Abstract This study aims to provide a basis for understanding the mechanisms of diurnal rainfall variability over Peninsular Malaysia by utilising the Non-Hydrostatic Regional Climate Model (NHRCM). The present day climate simulations at 5 km resolution over a period of 20 years, from 1st December 1989 to 31st January 2010 were conducted using the six-hourly Japanese re-analysis 55 years (JRA-55) data and monthly Centennial in situ Observation Based Estimates (COBE) of sea surface temperature as lateral and lower boundary conditions. Despite some biases, the NHRCM performed reasonably well in simulating diurnal rainfall cycles over Peninsular Malaysia. During inter-monsoon periods, the availability of atmospheric moisture played a major role in modulating afternoon rainfall maxima over the foothills of the Titiwangsa mountain range (FT sub-region). During the southwest monsoon, a lack of atmospheric moisture inhibits the occurrence of convective rainfall over the FT sub-region. The NHRCM was also able to simulate the suppression of the diurnal rainfall cycle over the east coast of Peninsular Malaysia (EC sub-region) and afternoon rainfall maximum over the Peninsular Malaysia inland-valley (IN sub-region) area during the northeast monsoon. Over the EC sub-region, daytime radiational warming of the top of clouds enhanced atmospheric stability, thus reducing afternoon rainfall. On the other hand, night-time radiational cooling from cloud tops decreases atmospheric stability and increases nocturnal rainfall. In the early morning, the rainfall maximum was confined to the EC sub-region due to the retardation of the north-easterly monsoonal wind by the land breeze and orographic blocking. However, in the afternoon, superimposition of the sea breeze on the north-easterly monsoonal wind strengthened the north-easterly wind, thus causing the zone of convection to expand further inland.

1 Introduction

Peninsular Malaysia, a unique landmass that protrudes southward from the Southeast Asian mainland, is surrounded by the South China Sea (SCS) to the east, and the Strait of Malacca and Andaman Sea to the west. With a strong thermal contrast between the surrounding seas and the land, and the presence of the Titiwangsa mountain range, which runs southward down the middle of the peninsula, Peninsular Malaysia is characterised by a number of uniquely shaped diurnal cycles (Richard 2010). Furthermore, the diurnal cycle over this region is also influenced by the monsoon cycle, which largely modulates the transport of moisture into the region. Detailed knowledge of the processes involved in shaping the diurnal cycle is fundamental in understanding the climate in any region. However, over this region, a limited number of process-

✉ Fredolin Tangang
tangang@ukm.my; ftangang@gmail.com

1   School of Environmental and Natural Resource Sciences, Faculty of Science and Technology, Universiti Kebangsaan Malaysia, 43600 Bangi, Selangor, Malaysia

2   Malaysian Meteorological Department, 46667 Petaling Jaya, Selangor, Malaysia

3   Ramkhamhaeng University Center of Regional Climate Change and Renewable Energy (RU-CORE), Bangkok, Thailand

4   Meteorological Research Institute, 1-1 Nagamine, Tsukuba, Ibaraki 305-0052, Japan

based studies have been carried out to understand the physical mechanisms involved in diurnal cycles. Hence, this study attempts to enhance understanding of the processes and mechanisms controlling diurnal cycles over Peninsular Malaysia.

The climate of Peninsular Malaysia is strongly modulated by the Asian-Australian monsoon and prevailing north-easterly winds from December to February (DJF), and south-westerly winds from June to August (JJA). Due to these nearly opposite prevailing winds over Peninsular Malaysia, the winter and summer monsoons are known locally as the northeast and southwest monsoon, respectively. Between these two monsoon seasons are the inter-monsoon periods. The annual cycles of rainfall are shaped by these monsoon cycles, along with strong topographical influences (Tangang et al. 2012). In general, Peninsular Malaysia can be divided into three regions: west coast, inland, and east coast, each with different diurnal rainfall cycles and peak phases (Ramage 1964; Nieuwolt 1968; Oki and Musiake 1994; Richard 2010). On the west coast during the inter-monsoon period, strong onshore breezes, due to the large land-sea temperature gradient, modulate strong convergence of moist air in the daytime with a maximum phase occurring in the afternoon–evening period. On the other hand, morning rainfall that is associated with a weather phenomenon is known as the Sumatra Squall Line (SSL; which is a squall line over the Strait of Malacca) which occurs over the west coast of the peninsula during boreal summer. This morning rainfall can be induced by the convergence of two cold and deep katabatic flows that were produced by the previous evening's precipitation systems over the east coast of northern Sumatra, and the west coast of the peninsula (Fujita et al. 2010). On the east coast of Peninsular Malaysia, during the months of November to January, the convective activity over the southern portion of the South China Sea is modulated by long-period synoptic forcing, such as monsoon surges and easterly waves (e.g. Chang et al. 2005; Tangang et al. 2008; Chen et al. 2013), and is also significantly influenced by diurnal forcing. The offshore breeze that converges with the north-easterly monsoon wind generates offshore convection, which develops into an organised precipitation system. Although the diurnal cycle during winter is relatively less prominent compared to that during boreal summer, this diurnal convection persists in the region regardless of whether the synoptic-scale forcing is weak or strong (Lim 1979).

Despite this general understanding, the previous studies on diurnal rainfall characteristics and mechanisms over Peninsular Malaysia are limited. Most works have either focused on a particular area, season, or yearly averages using limited rain-gauge stations or coarse-resolution satellite observation data (Ramage 1964; Nieuwolt 1968;

Oki and Musiake 1994; Kikuchi and Wang 2008; Fujita et al. 2010). In general, using rain-gauge data, most studies showed consistent results of diurnal rainfall cycle varying spatially and temporally. However, these studies failed to describe the physical and thermodynamic mechanisms that contributed to the variations. The difficulties in examining the physical and thermodynamic mechanisms of diurnal rainfall variability over Peninsular Malaysia arose from the lack of reliable sub-daily surface and atmospheric observations. Radiosonde data can be used to better understand the mechanisms related to the diurnal cycle (Sun et al. 2010); however, the number of radiosonde data sets of a sufficiently long timespan and sufficiently high spatial and temporal density for quantifying the highly localised nature of the diurnal cycle over Peninsular Malaysia is very limited. Therefore, a regional climate model (RCM) is a viable tool for investigating the physical mechanisms and processes related to diurnal cycles.

During the past few years, the number of studies utilising RCMs has increased dramatically, both for simulation of current regional climate and projections of future climate up to the end of the 21st century (e.g. Giorgi et al. 2004a, b; Räisänen et al. 2004; Van Phan et al. 2014; Cruz et al. 2016; Juneng et al. 2016; Loh et al. 2016). Over the Maritime Continent, the current RCMs are operated at horizontal resolutions of 25 km to 50 km (e.g., Raghavan et al. 2015; Cruz et al. 2016; Juneng et al. 2016; Kieu-Thi et al. 2016; Loh et al. 2016; Ngo-Duc et al. 2016; Chung et al. 2017; Cruz and Sasaki 2017; Ratna et al. 2017). Although at this resolution, the main characteristics of the monsoon climate can be captured, the physiographical characteristics due to complicated mountain systems and surrounding seas, as well as small islands, cannot be adequately resolved in the RCMs (e.g. Van Phan et al. 2014; Raghavan et al. 2015; Cruz et al. 2016; Juneng et al. 2016). Therefore, to resolve the mechanisms of rainfall diurnal variability over the region, the horizontal resolution of RCMs must be sufficiently high. This can be achieved by multiple nesting and application of a non-hydrostatic model with a resolution of <5 km to capture the complex physiography and associated processes (e.g., Argüeso et al. 2016; Hassim et al. 2016).

2 Methodology

2.1 RCM setup

This study utilised the non-hydrostatic regional climate model (NHRCM), which was developed based on the operational Non-Hydrostatic Model (NHM) of the Meteorological Research Institute (MRI) and the Numerical Prediction Division of the Japan Meteorological Agency

(NPD/JMA) (Saito et al. 2006; Sasaki et al. 2008). NHRCM is a climate version of the JMA-NHM. This model has not been previously used for any simulation over Peninsular Malaysia. Physical parameterisations used in this study followed those of Nakano et al. (2012) and Cruz et al. (2016). The MRI-JMA Simple Biosphere Model (Hirai and Ohizumi 2004) was used to describe the surface processes in the model. A spectral nudging scheme based on the spectral boundary coupling method of Kida et al. (1991) and Sasaki et al. (2000) was used in simulations. The scheme preserves the large-scale field (long-wave component) of the boundary conditions within the nested inner domain in wavenumber space, which consequently improves model performance (Yasunaga et al. 2005). The model performance is also dependent on the cumulus parameterisation scheme (CPS) used in the model (e.g. Wang et al. 2007; Koo and Hong 2010; Fersch and Kunstmann 2013; Choi et al. 2015). The previous studies showed that without a CPS (at 5 km resolution), the NHRCM overestimated intense rainfall and underestimated weak-to-moderate rainfall (Saito et al. 2007; Sasaki et al. 2008). Therefore, a revised version of the Kain–Fritsch (KF) CPS was used in the NHRCM setup for this study. The KF CPS is a mass flux type parameterisation commonly used in mesoscale models and over the Southeast Asia region (Kain 2004; Saito et al. 2006; Evans and Westra 2012; Yang et al. 2014; Raktham et al. 2015; Bhatt et al. 2016; Cruz et al. 2016). The revision made to the CPS was to suppress the false predictions of rainfall areas along coastlines during the warm season. This is achieved by modifying the level of the updraft source layer when assessing the activation of the scheme. In addition, the revised KF CPS was modified to lower the consumption of CAPE during convection (e.g., 70% compared to 90% in normal KF CPS) and allow the remaining CAPE to influence the next convection process (e.g., Cruz et al. 2016).

The simulation was carried out in a one-way nesting configuration, with the coarser mother domain of 20 km resolution covering a region of 5°S–15°N and 92°E–120°E (hereafter NHRCM20). The finer child domain of 5 km resolution covers an area of 2°S–10°N and 96°E–110°E (hereafter NHRCM05; Fig. 1). The simulation was run over a period of 20 years, from 1st December 1989 to 31st January 2010. For model spin-up, the first month of the simulation was discarded. The simulation was forced by 6-hourly Japanese re-analysis 55 years (JRA-55) data with a resolution of 1.25° (Kobayashi et al. 2015; Kobayashi and Iwasaki 2016). The monthly Centennial in situ Observation Based Estimates (COBE) sea surface temperature (Ishii et al. 2005) version 1.5, with a resolution of 1.0°, was used as the sea surface temperature lower boundary condition. The NHRCM model was run at 60 vertical levels with the model top at 0.1 hPa.

2.2 Observational data

Prior to the investigation of diurnal rainfall variability over Peninsular Malaysia, NHRCM05's capability in simulating seasonal mean of rainfall and surface temperature was evaluated based on the 0.05° resolution gridded daily data set of Wong et al. (2011). This data set spans from 1976 to 2006, was derived from the daily rainfall and surface temperature observation network, and consisted of 123 stations that spread across Peninsular Malaysia (e.g. Mohd et al. 2015; Wong et al. 2016). However, only data for a period of 17 years from 1990 to 2006 were used in this study.

The ability of NHRCM05 to reproduce diurnal rainfall cycle characteristics over land was validated using hourly rainfall, surface air temperature, and global solar radiation data from 24 surface meteorological stations (Fig. 1b) that span a period of 20 years from 1990 to 2009. The names and locations of these stations are listed in Table 1. Rainfall data from these stations were collected using a combination of Dines pluviographs and tipping-bucket rain gauges. A threshold of 0.1 mm/h was used to define rainfall occurrences (Evans and Westra 2012). The use of station-based data is justified due to the lack of high-quality gridded data that can be used to validate model results. For the validation of NHRCM05, precipitation over the Malacca Straits, Tropical Rainfall Measuring Mission (TRMM) 3B42 version 7 satellite data was used (Huffman et al. 2007). However, the TRMM data are only available from 1998 to 2015, and its resolution is rather coarse (25 km). The vertical structure of the NHRCM05 atmosphere was evaluated using radiosonde data from five upper air stations with ascents at 08:00 and 20:00 Malaysian Standard Time (MST). The MST precedes the Coordinated Universal Time (UTC) by 8 h. Radiosonde data used in this study were of 4-s intervals, extending from the ground surface to the top of atmosphere. However, prior to the year 2000, only data at standard and significant pressure levels (Ramella Pralungo et al. 2014) were available.

2.3 Data analyses

Data analyses were conducted on a seasonal basis, with seasons defined as the northeast monsoon [December–February (DJF)], the first inter-monsoon period [March–May (MAM)], the southwest monsoon [June–August (JJA)], and the second inter-monsoon period [September–November (SON)]. The radiosonde data were first rounded up to the nearest 10 hPa before being seasonally averaged. For comparison with NHRCM05 model data, the lowest level of radiosonde data was truncated at 1000 hPa. Following the topography, we regionalised Peninsular Malaysia into four diurnal sub-regions, namely: west coast (WC; coastal area of west Peninsular Malaysia), central mountain range
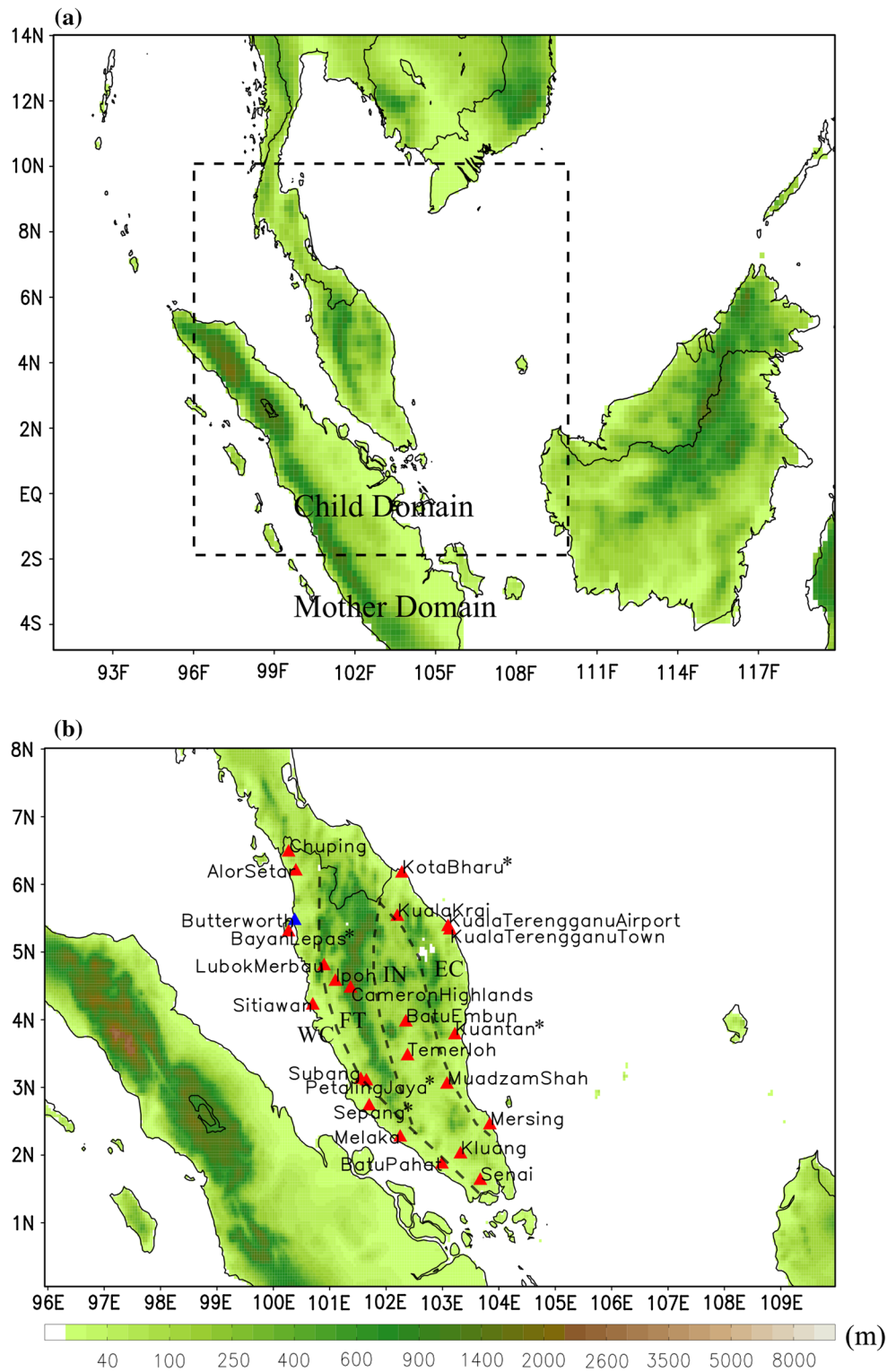
Fig. 1 **a** Map of mother domain (NHRCM20) and child domain (NHRCM05) with model orography of 20 km resolution. **b** Locations of the meteorological stations used in this study with model orography of 5 km resolution. Rainfall diurnal cycle over Peninsular Malaysia is divided into four different sub-regions: WC (coastal area of west Peninsular Malaysia), FT (foothills of Titiwangsa range), IN (inland-valley area), and EC (coastal area of east Peninsular Malaysia). *Red triangle* indicates station situated on a land pixel, while *blue triangle* indicates station on an ocean pixel in the NHRCM simulation

Table 1 List of the four sub-regions with information on meteorological station name, indicator, location, and elevation

Sub-region	Station name	Station indicator	Location	Elevation (m)
WC	Bayan Lepas	48601	5.30N 100.27E	2.4
	Butterworth	48602	5.47N 100.38E	3.3
	Alor Setar	48603	6.20N 100.40E	3.9
	Chuping	48604	6.48N 100.27E	21.7
	Sitiawan	48620	4.22N 100.70E	6.7
	Sepang	48650	2.73N 101.70E	16.1
	Melaka	48665	2.27N 102.25E	8.5
	Batu Pahat	48670	1.87N 102.99E	6.3
WM	Lubok Merbau	48623	4.80N 100.90E	77.5
	Ipoh	48625	4.57N 101.10E	50.1
	Cameron Highlands	48632	4.47N 101.37E	1545.0
	Subang	48647	3.12N 101.55E	26.6
	Petaling Jaya	48648	3.10N 101.65E	60.8
IN	Batu Embun	48642	3.96N 102.35E	49.5
	Temerloh	48653	3.46N 102.38E	39.1
	Muadzam Shah	48649	3.05N 103.08E	33.3
	Kluang	48672	2.02N 103.32E	88.1
	Senai	48679	1.63N 103.67E	37.8
EC	Kota Bharu	48615	6.17N 102.28E	4.36
	Kuala Krai	48616	5.53N 102.20E	58.3
	Kuala Terengganu Airport	48618	5.38N 103.10E	5.2
	Kuala Terengganu Town	48619	5.33N 103.13E	35.1
	Kuantan	48657	3.78N 103.22E	15.23
	Mersing	48674	2.45N 103.84E	43.6

(FT; foothills of Titiwangsa range), inland-valley (IN), and east coast (EC; coastal area of east Peninsular Malaysia) (Fig. 1b). Table 1 lists the stations included in each sub-region. This regionalisation is similar to those of previous studies (e.g. Ramage 1964; Nieuwolt 1968; Oki and Musiake 1994; Richard 2010), except the new FT sub-region classification, which covers both sides of the Titiwangsa mountain range. The creation of this sub-region allows the effect of the mountain range on the rainfall diurnal cycle to be isolated and better understood. For calculating the average values of simulated parameters over a particular sub-region, model outputs of the grid box where the station is located were aggregated. In cases where more than one station appeared in a particular grid box, the value of that grid box was counted more than once, according to the number of stations.

The analysis focuses on two rainfall parameters, namely amount and frequency. Following Zhou et al. (2008), we defined rainfall amount (intensity) as the accumulated rainfall amount for every hour (precipitating hour). Rainfall frequency is defined as the percentage of days when hourly rainfall exceeds 0.1 mm/h. Vertically integrated moist static energy (MSE), convective available potential energy (CAPE), and convective inhibition energy (CIN) over the

entire child domain were calculated as indicators of convective precipitation simulated by NHRCM05. The MSE is defined as the sum of the sensible, latent, and geopotential energy, and is expressed as follows:

$$MSE = C_pT + Lq + gZ$$

where C_p is the specific heat of air at constant pressure, T is the air temperature, L is the latent heat of evaporation, q is the specific humidity, g is the acceleration due to gravity, and Z is the height (Im et al. 2008). For the calculation of CAPE and CIN, the Grids Analysis Display System (GrADS) "plotskew" function, developed by Robert Hart of Pennsylvania State University available at (http://moe.met.fsu.edu/~rhart/skew.html), was used.

3 Evaluation of model performance

3.1 Seasonality of the daily rainfall and surface temperature

Figures 2 and 3 compare the seasonal rainfall and surface temperature spatial distributions of NHRCM05 and gridded data over Peninsular Malaysia. In general, NHRCM05
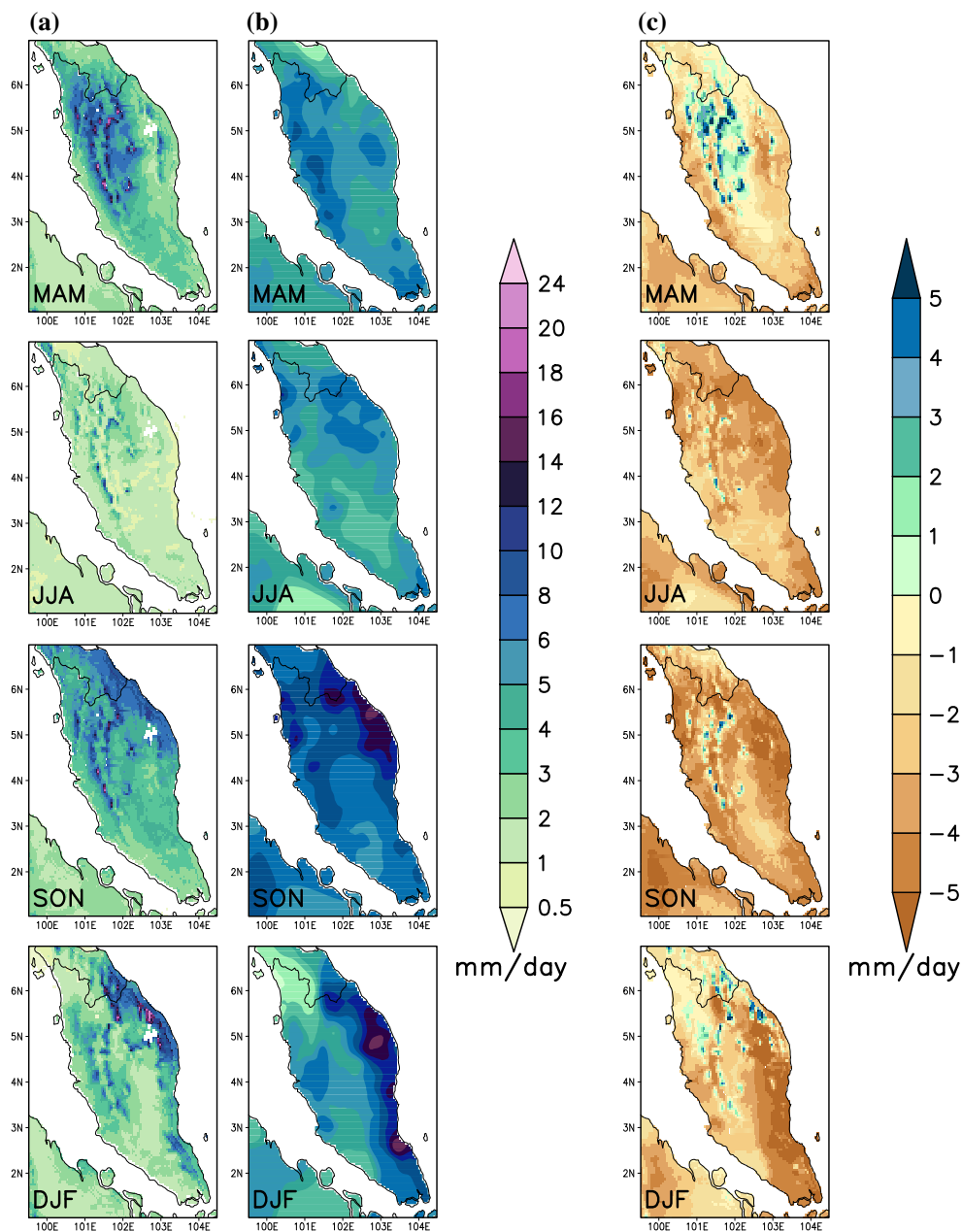
Fig. 2 Seasonal mean of daily average rainfall (mm/day) **a** simulated by NHRCM05, **b** observed by gridded data, and **c** biases between simulated rainfall and gridded data

simulated the spatial variation of both seasonal rainfall and surface temperature throughout Peninsular Malaysia rather well. In the EC sub-region, the higher amount of rainfall during Dec–Feb (DJF) and Sept–Nov (SON) was reasonably simulated by NHRCM05. Similarly, NHRCM05 simulated the spatial pattern and amount of rainfall during inter-monsoon periods (MAM and SON) over the WC and FT sub-regions. Much like in the observations, the relatively drier conditions throughout Peninsular Malaysia during JJA were also featured in NHRCM05. However, NHRCM05 tended to produce a wet bias over mountainous areas and a dry bias in the coastal region throughout the seasons. Underestimation of the rainfall amount by NHRCM05 in the coastal region compared to the gridded rainfall data may likely be attributed to the forcing field itself (e.g., Francisco et al. 2006). Ceglar et al. (2017) had shown that JRA55 reanalyses data generally underestimated rainfall amount compared to observation over the Peninsular Malaysia. Noticeably, Fig. 2 shows that gridded observed rainfall data tended to have overly smooth and unrealistic rainfall pattern over the mountainous area, compared to that of the NHRCM05. This may be due to
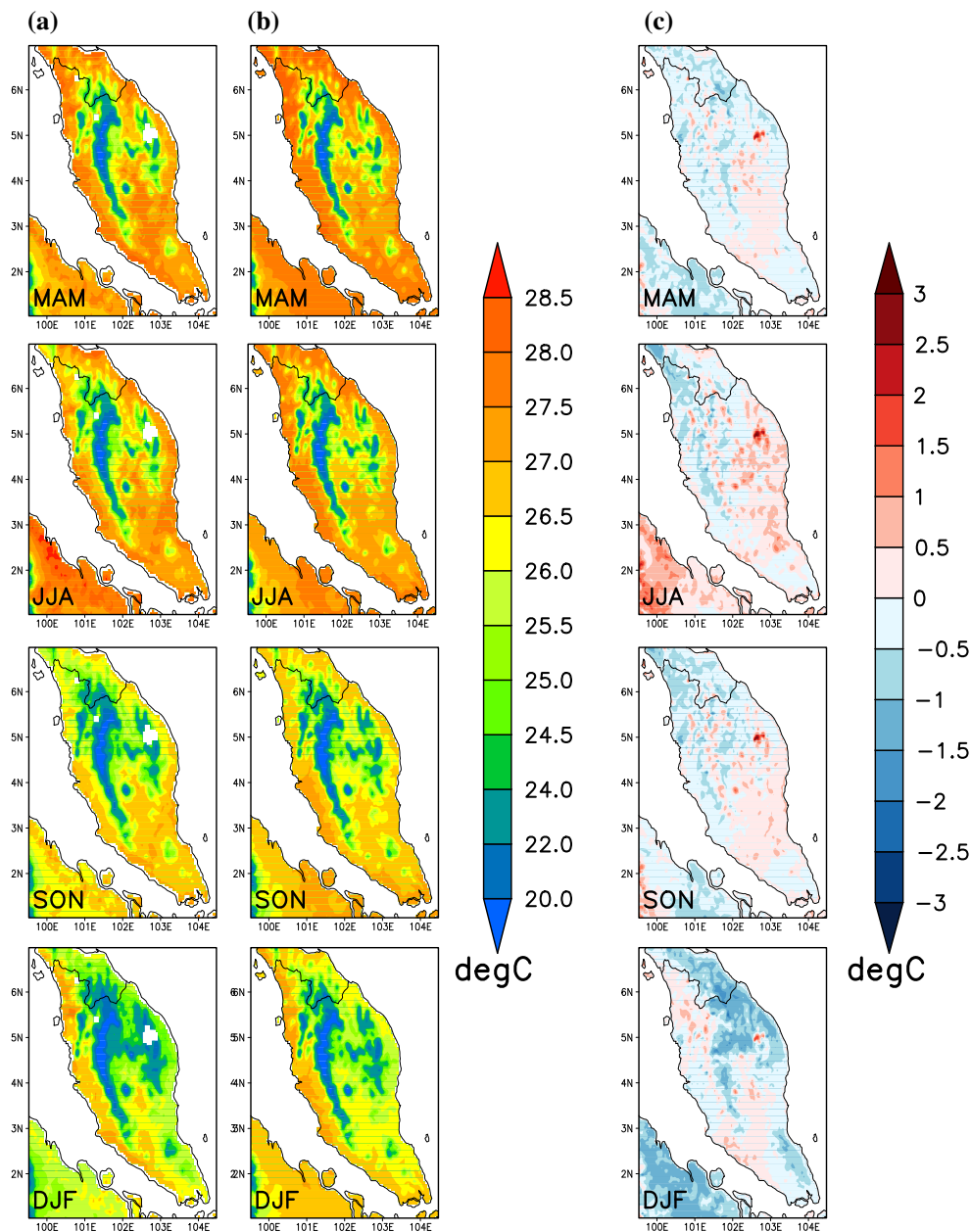
Fig. 3 Seasonal mean of daily averaged surface air temperature (°C) **a** simulated by NHRCM05, **b** observed by gridded data, and **c** biases between simulated surface air temperature and gridded data

limited meteorological stations over the highland and inland areas, thus producing less reliable interpolated data over this sub-region. In general, the performance of NHRCM05 in simulating the seasonal rainfall was consistent with that of the PRECIS modelling system described in Kwan et al. (2014).

The distinct contrast of temperature during DJF ($\sim$24–26 °C) and MAM ($\sim$26–28 °C) because of advection of cold air from the north during DJF, and also increased insolation due to the sun position directly above

Peninsular Malaysia during MAM, was also captured well by NHRCM05 (Fig. 3). The biases ranged from −2 to 2 °C with a tendency for cold (warm) bias over the east coast of Peninsular Malaysia during DJF (JJA) and cold (warm) bias over the west coast of Peninsular Malaysia during JJA (DJF). Such magnitudes of biases are comparable to those of the PRECIS model (biases <2 °C; Kwan et al. 2014) and the Regional Climate Model version 4.3 (RegCM4.3) (biases of −3 to 3 °C; Cruz et al. 2017) over Peninsular Malaysia.

3.2 Large-scale features

In general, both the forcing field (JRA55) and the NHRCM simulated large-scale circulations are remarkably consistent (Fig. 4). In both the JRA55 and NHRCM simulations, the spatial distribution of mean sea-level pressure (MSLP) depicts low pressure in the Borneo island and a prominent "pressure surge" (represented by 1009.5–1011.5 hPa contour), which is a common pattern of MSLP during DJF over the region (Fig. 4l, p). However, the simulated low-pressure system over Borneo, which is associated with the Borneo vortex, tended to be slightly stronger compared to JRA55. The low-level tropospheric wind over the SCS, which is often accompanied by cold surges from the north and moisture from the north-western Pacific Ocean (Tangang et al. 2008; Ooi et al. 2011), was also well modelled in the NHRCM simulation (Fig. 4d). Accordingly, the Borneo vortex and cold surge features in NHRCM were consistent compared to JRA55, except that the moisture tended to be concentrated over the vortex region. During JJA, the NHRCM also simulated well prominent features over the region, including the south-westerly monsoonal

wind, relatively high MSLP, and reduced moisture compared with other seasons, consistent with the JRA55. The consistency between the two also continued during the inter-monsoon periods, in which both featured weak low-level tropospheric winds (Fig. 4a, c, e, g).

4 Diurnal features

4.1 Seasonality of the diurnal rainfall amount and frequency

The diurnal rainfall amount over Peninsular Malaysia varies depending on the season and location, and was previously classified into three distinct sub-regions (Ramage 1964; Nieuwolt 1968; Oki and Musiake 1994; Richard 2010). As described in Sect. 2.3, the FT sub-region was introduced to allow a better understanding of the roles of mountain ranges in modulating the diurnal cycle. In terms of rainfall hourly amount, it was found that the homogeneity of stations within each sub-region is still maintained and consistent with the previous studies
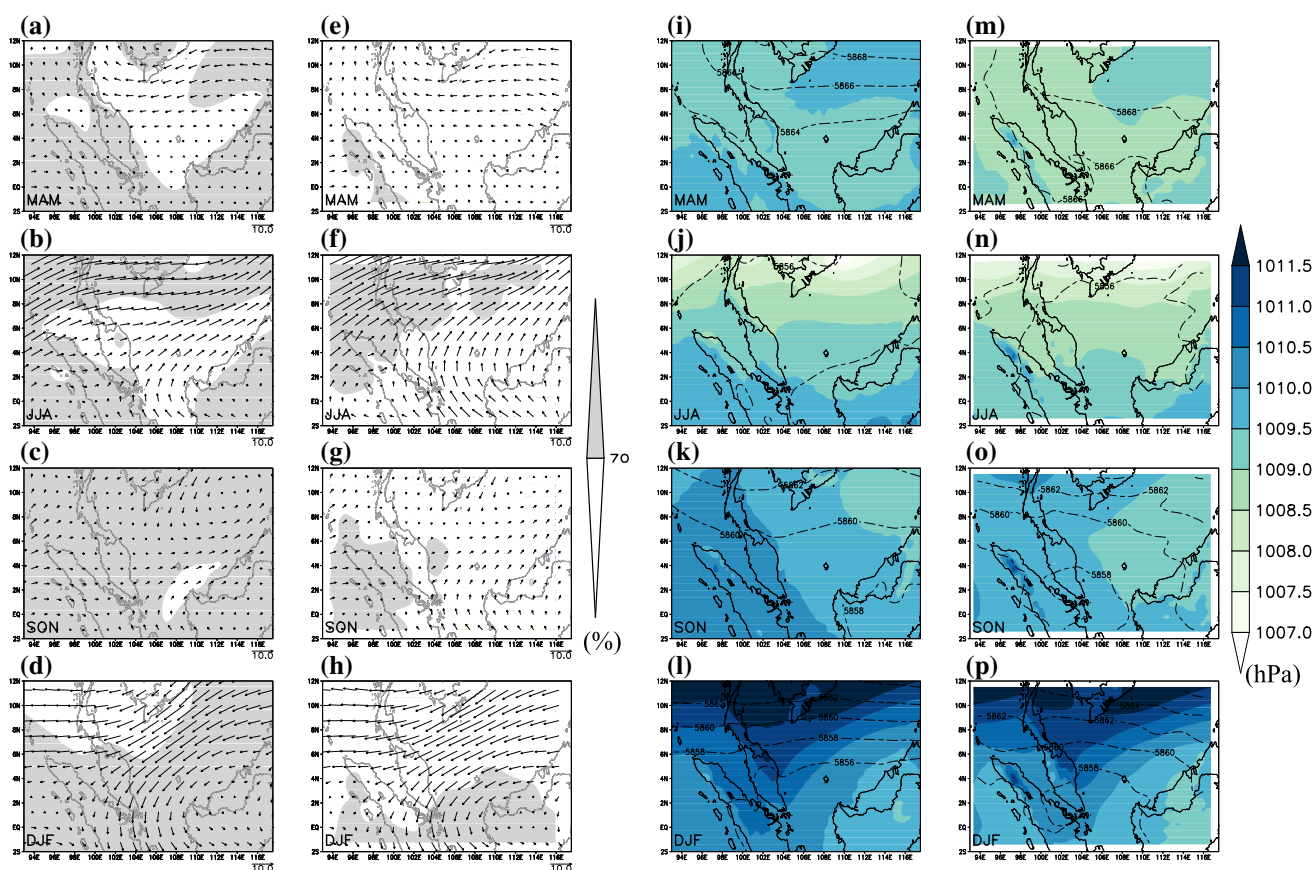

Fig. 4 Seasonal mean of large-scale features for **a–d** wind (*arrow*) and relative humidity (%, *shaded*) at 850 hPa from JRA55 data set and **e–h** simulated by NHRCM, **i–l** 500 hPa geopotential height (gpm, *dashed line*) and mean sea-level pressure (hPa, *shaded*) from JRA55 data set and **m–p** simulated by NHRCM

using fewer sub-regions (not shown). Hence, subsequent discussion of diurnal variability of rainfall and surface temperature over Peninsular Malaysia will be based on sub-region averages.

Prior to discussing the physical mechanisms that contribute to diurnal rainfall variability, the regional and seasonal aspects of diurnal rainfall cycles over Peninsular Malaysia are briefly discussed. During the northeast monsoon, the EC sub-region received the heaviest rainfall due to its full exposure to the moist and strong north-easterly monsoonal winds crossing the South China Sea. Consistent

rainfall of more than 0.4 mm/h was recorded throughout the entire day (Fig. 5p). Over the IN sub-region, there was light rain in the morning (less than 0.2 mm/h), which became heavy in the afternoon–evening period (Fig. 5l). In contrast, over the leeward side of the Titiwangsa range, the diurnal rainfall was low compared to the east of Peninsular Malaysia. This is due to the drying of the north-easterly wind after crossing over the Titiwangsa mountain range (Lim 1979). However, rainfall over the west of Peninsular Malaysia (WC and FT sub-regions) occurred mainly in the afternoon and evening (Fig. 5d, h).
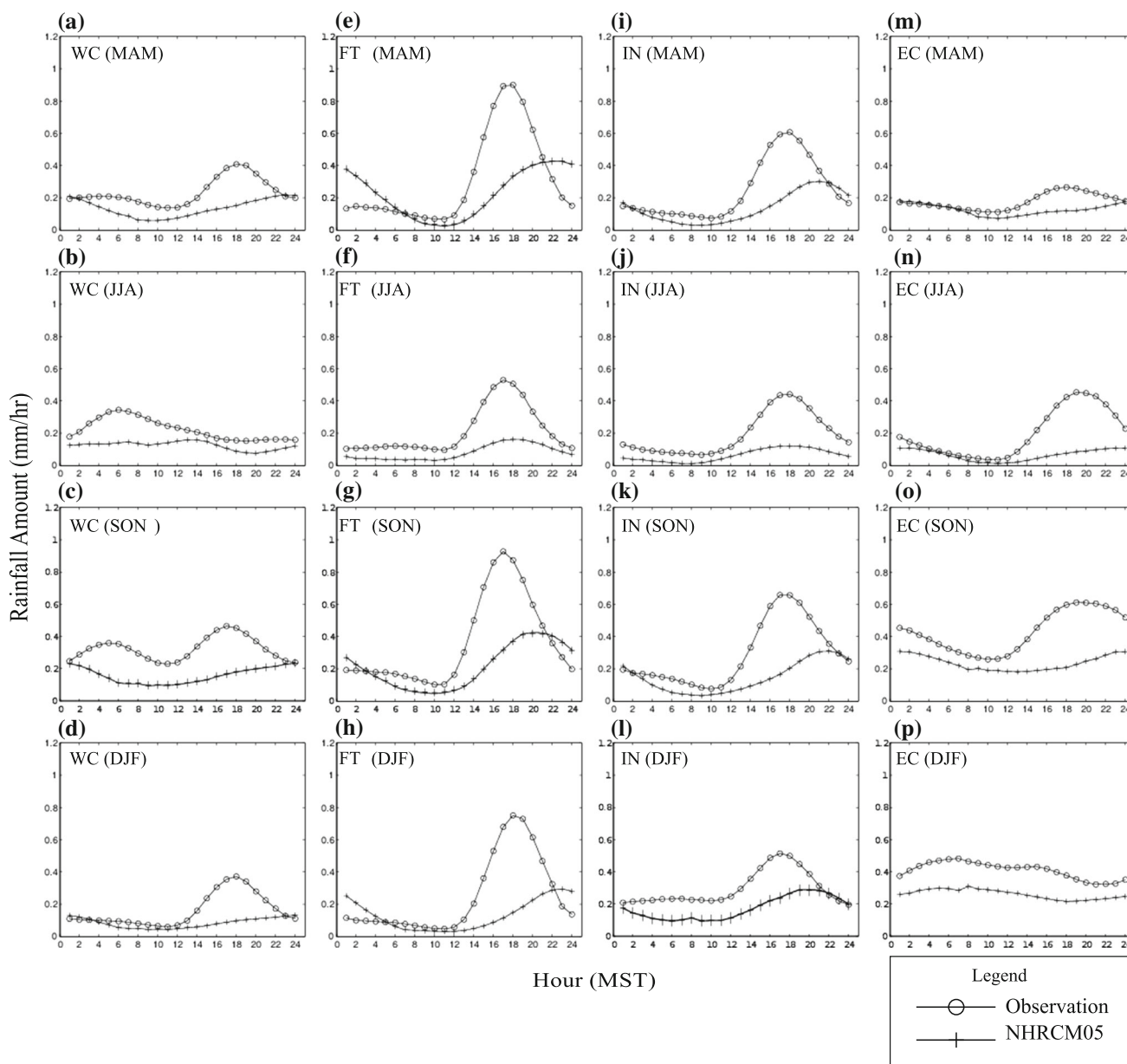

Fig. 5 Diurnal cycle of hourly rainfall amount in the four classified sub-regions according to season. The *line of closed circles* represents rain-gauge data, while the *line of crosses* represents the NHRCM05 simulation. The *rows* represent different seasons, while the *columns* stand for the four, representative, diurnal sub-regions

In the early morning (02:00 MST to 09:00 MST) during the southwest monsoon, the maximum morning rainfall occurred over the WC sub-region (Fig. 5b). For the FT sub-region, which is located further inland (>50 km from the coastline of west Peninsular Malaysia), this morning rainfall maximum was not experienced (Fig. 5f). The WC/FT maximum morning rainfall pattern was largely determined by the eastward-traveling SSL, which became disorganised and dissipated once it made landfall in the coastal area (Lo and Orton 2016). In contrast, over the leeward side of the Titiwangsa range, the rainfall occurred during the late afternoon–evening period. However, the afternoon–

evening rainfall over the IN and EC sub-regions was comparatively less heavy than that of the northeast monsoon rainfall (Fig. 5j, n).

During inter-monsoon periods (MAM and SON), the FT sub-region was exposed to strong local convection systems, and thus, the afternoon rainfall was the heaviest with more than 1.0 mm/h of rainfall recorded in between 15:00 MST and 19:00 MST (Fig. 5e, g). In comparison, for the WC and IN sub-regions, although afternoon rainfall maxima occurred during both the inter-monsoon periods, the rainfall amount was much lower (less than 0.6 mm/h) than in the FT sub-region (Fig. 5a, c, i, k). Interestingly, for the EC
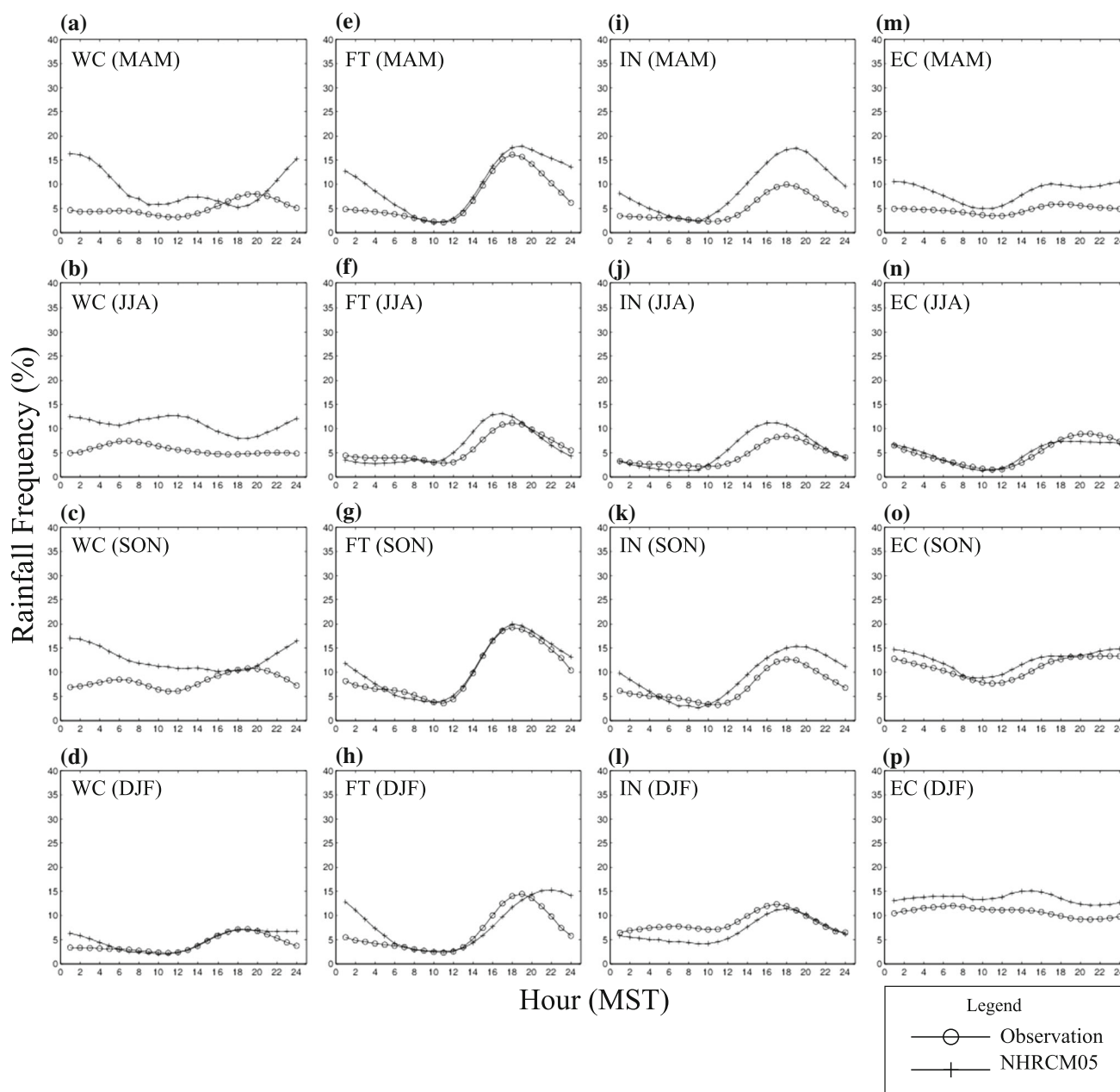

Fig. 6 As in Fig. 5 except for hourly rainfall frequency

sub-region, afternoon rainfall maxima only occurred during SON (Fig. 5o). The dry conditions over the EC sub-region during MAM were largely attributed to the occurrence of cross-equatorial flow that transports moisture from the region to areas south of equator (Siew et al. 2014; Loh et al. 2016).

Figures 5 and 6 also provide comparisons between the observed and modelled diurnal cycles of hourly rainfall amount and frequency according to season for the four classified sub-regions. The rainfall intensity generally had similar characteristics (e.g., afternoon and morning rainfall peak phase) to that of the rainfall amount (not shown). Hence, subsequent discussion will only be based on the rainfall amount and frequency. Overall, the NHRCM05 shows reasonably good performance in simulating the general characteristics of diurnal rainfall. However, the underestimation of rainfall amount is notable. Over the WC sub-region, NHRCM05 reasonably simulated maximum afternoon rainfall amount and frequency during both inter-monsoon periods (Figs. 5a, c, 6a, c). However, the NHRCM05 simulation did not adequately capture morning rainfall over the region during the southwest monsoon and SON (Figs. 5b, c, 6b, c). Over the FT sub-region, maximum afternoon rainfall amount and frequency were simulated well by NHRCM05 during the inter-monsoon periods. However, the peak time for rainfall maximum amount over the FT sub-region was delayed by 2 h compared with observations. Nevertheless, the simulated maximum afternoon rainfall amount was relatively weak (<0.4 mm/h) and the duration was prolonged from 18:00 MST to 24:00 MST (Figs. 5e, g, 6e, g). Over the IN sub-region, NHRCM05 reasonably simulated the afternoon rainfall maximum amount and frequency throughout the entire year (Figs. 5i–l, 6i–l). Furthermore, the occurrence of rainfall throughout the entire day during the northeast monsoon in the IN sub-region was also captured well by NHRCM05 (Fig. 5l). Over the EC sub-region, NHRCM05 was able to capture the suppression of the diurnal rainfall cycle during the northeast monsoon but with lower rainfall amounts compared to the observations (Figs. 5p, 6p).

The ability of NHRCM05 to simulate seasonal diurnal rainfall cycles was evaluated using the correlation coefficient (r) and root-mean-square error (RMSE) (Table 2). Overall, the r values for diurnal rainfall amount and frequency over the inland area (FT and IN sub-regions) and diurnal rainfall frequency over the EC sub-region were moderate (>0.3; p value <0.05, i.e., significant at the 95% level), demonstrating that the NHRCM05 substantially captured the climatology of the diurnal rainfall cycle over the region. Over the inland area (FT and IN sub-regions), the r values of diurnal rainfall amount were high during the southwest monsoon (>0.6; p value <0.05) and moderate during other seasons. However, the RMSE was

Table 2 Correlation coefficients (r) and root-mean-square error (RMSE) between the observed and simulated NHRCM05 diurnal rainfall amount and frequency

Sub-region	Season	Amount (mm/h)		Frequency (%)	
		r	RMSE	r	RMSE
WC	MAM	0.38	0.16	0.35	4.5
	JJA	0.37	0.16	0.06	3.8
	SON	0.30	0.21	0.09	4.2
	DJF	0.53*	0.15	0.14	2.5
FT	MAM	0.44*	0.38	0.92*	4.5
	JJA	0.88*	0.23	0.89*	3.1
	SON	0.54*	0.38	0.94*	3.6
	DJF	0.34	0.32	0.12	4.6
IN	MAM	0.50*	0.23	0.92*	5.0
	JJA	0.87*	0.21	0.93*	2.2
	SON	0.42*	0.28	0.88*	3.4
	DJF	0.37	0.29	0.40*	4.4
EC	MAM	0.26	0.13	0.78*	3.9
	JJA	0.65*	0.21	0.84*	2.7
	SON	0.23	0.27	0.90*	4.7
	DJF	0.39	0.22	0.43*	4.4

*The statistical significance of correlation coefficients for diurnal rainfall amount and frequency are calculated at 95% confidence level using a Student's t test

generally higher in all seasons compared to other sub-regions. On the other hand, over the coastal area (WC and EC sub-regions), the r values of the diurnal rainfall amount were mostly weak (~ 0.3). However, during the southwest (northeast) monsoon, the r value was significant and moderate over the EC (WC) sub-region. The r values of diurnal rainfall frequency were mostly strong (>0.6; p value <0.05) in all seasons over the inland areas and EC sub-region, but weak over WC sub-region. However, there was a mixed performance of diurnal rainfall frequency RMSE patterns simulated in the inland and coastal areas.

Earlier studies over the Maritime Continent have indicated that a common problem in regional climate models is too frequent rainfall at a reduced amount (e.g., Gianotti et al. 2012; Ngo-Duc et al. 2016; Chung et al. 2017). However, based on the diurnal rainfall frequency shown in Fig. 6 and Table 2, NHRCM05 appears to perform better than earlier studies in simulating the rainfall frequency. TRMM had shown an average of 30% daily rainfall frequency over Peninsular Malaysia, but the frequency was doubled in RegCM (e.g., Gianotti et al. 2012; Chung et al. 2017). A similar result was obtained by Ngo-Duc et al. (2016) when the simulated values by RegCM were compared with rain-gauge data. On the

other hand, NHRCM05 seemingly did not overestimate the rainfall frequency at all hours over most of the sub-regions (Fig. 6; Table 2). This good performance by the model in simulating the frequency could be attributed to its ability to represent the regional-scale processes, such as atmospheric circulation and moisture transport (e.g. Iorio et al. 2004; Sun et al. 2006). The high spatial resolution also allows local processes to be captured well by the model (e.g., orographic lifting over the foothills of the mountain range).

4.2 Seasonality of the surface temperature diurnal cycle

Figure 7 shows the comparison of the observed versus simulated diurnal cycle of 1.5 m air temperature. Compared with rainfall, the NHRCM05 performance in simulating general characteristics of the diurnal temperature cycle was far better. Throughout the sub-regions, the afternoon mean maximum temperatures simulated by NHRCM05 were about 2 °C lower than the observations
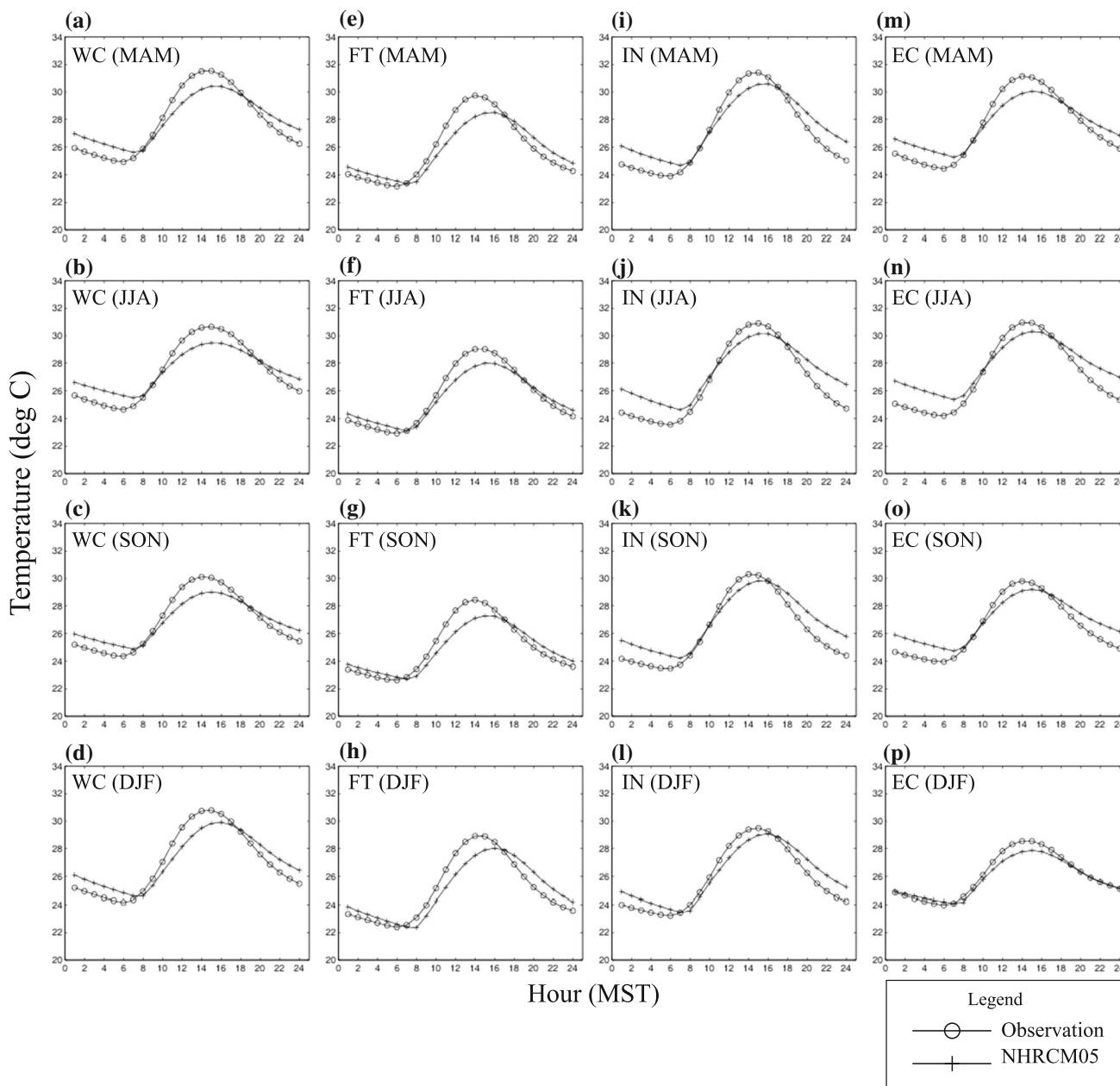
Fig. 7 As in Fig. 5 except for hourly surface temperature

during the southwest monsoon and inter-monsoon periods. During the northeast monsoon, biases were reduced and the simulated mean maximum temperature was less than 1 °C cooler than the observations (Fig. 7d, h, l, p). Similarly, the performance of NHRCM05 was better when simulating the morning mean minimum temperature. Throughout the sub-regions, the morning mean minimum temperature simulated by NHRCM05 was 1 °C higher than the observations during the southwest monsoon and inter-monsoon periods, and was equal for the northeast monsoon (Fig. 7d, h, l, p). It is also noted that maximum and minimum temperatures were relatively lower in the FT sub-region, since one of the stations was located at a higher elevation (Cameron Highlands is about 1545 m above sea level).

Despite good performances of NHRCM05 in simulating the surface temperature, there were shortcomings including notable warm and cold biases in the morning and afternoon, respectively, as well as the delayed phase of the afternoon temperature peak. These systematic biases could be related to the overestimation of the cloud amount. Compared to global solar radiation, which was measured with pyranometers at meteorological stations, the NHRCM05 simulated less surface solar radiation at 09:00 MST (observed 173 vs. simulated 113 W/m^2; averaged over all sub-regions and seasons), indicating "cloudy skies" over the sub-regions. The 09:00 MST was taken as a representative time of surface solar radiation given the minimum convection over land that provides a condition without the presence of complicated convective clouds (e.g., Lim 1979; Birch et al. 2016). In the afternoon, due to less solar radiation to warm land surface, less surface sensible and latent heat flux was simulated by NHRCM05 (Fig. 8). This in turn causes weak vertical mixing resulting in the delay in atmospheric boundary layer warming. As a result, the afternoon temperature was underestimated and the peak lagged (Fig. 7). In addition, delayed peak phase of afternoon temperature may also affect the peak phase of afternoon maximum rainfall amount. A delayed of ∼2 h of simulated afternoon temperature than observation (Fig. 7e, g) was consistent with a delayed of ∼2 h of simulated afternoon rainfall maximum amount (Fig. 5e, g). On the other hand, "cloudy skies" prevent radiative cooling of land surface during morning (before sunrise), resulting in overestimation of temperature (Fig. 7).

4.3 Seasonality of the atmospheric mean profiles

Atmospheric profiles contain important information on the build-up of the boundary layer and the triggering of moist convection. The mean vertical structure of the atmosphere in late afternoon (20:00 MST) throughout all seasons was evaluated at five radiosonde stations, namely Bayan Lepas and Sepang (located in the WC sub-region), Petaling Jaya
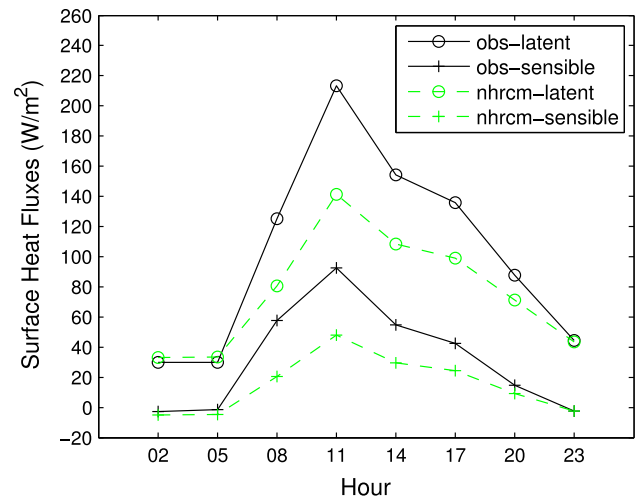

Fig. 8 Diurnal cycle of 3-hourly surface heat fluxes (W/m^2), averaged over all sub-regions and seasons. The *line of black-circles* represents latent heat flux, while black-crosses represent sensible heat flux from JRA55 data set. The *dashed line of green-circles* represents latent heat flux, and *green-crosses* represent sensible heat flux, simulated by NHRCM05

(located in the FT sub-region), and Kota Bharu and Kuantan (located in the EC sub-region). In general, the biases of NHRCM05 simulated profiles appeared to be consistent across stations and seasons. Figure 9 shows the profiles of three representative stations during MAM and JJA as examples. Consistently throughout the stations and seasons, NHRCM05 produced warmer lapse rates above 400 hPa compared with observations. Furthermore, the simulated profiles also indicated higher dew point lapse rates compared with the observations.

The atmospheric profiles in Fig. 9 suggest that the potential mechanisms for overestimation of rainfall frequency (as shown in Fig. 6e, f, m) by NHRCM05 could be mostly related to excessive moisture at the boundary layer. This excess moisture can be caused by orographic lifting due to the prevalence of a moist westerly (easterly) sea breeze towards the high terrain in west (east) coast of Peninsular Malaysia. This condition eventually weakens CIN, causing air parcels to be more buoyant, thus facilitating the triggering of convection (Mapes 2000; Mori et al. 2004; Brockhaus et al. 2008; Im et al. 2008; Myoung and Nielsen-Gammon 2010). Figure 9 also suggests that the simulated convective rainfall was less intense, mostly related to the weak simulated CAPE. A warm bias of about 1–3 °C in the upper tropospheric layer (above 400 hPa) caused the upper tropospheric layer in the model to be more stable than observations (Fig. 9). Hence, the updrafts within the convective towers were weaker in the model, lowering the CAPE and thus weakening the convective system (e.g., Myoung and Nielsen-Gammon 2010).
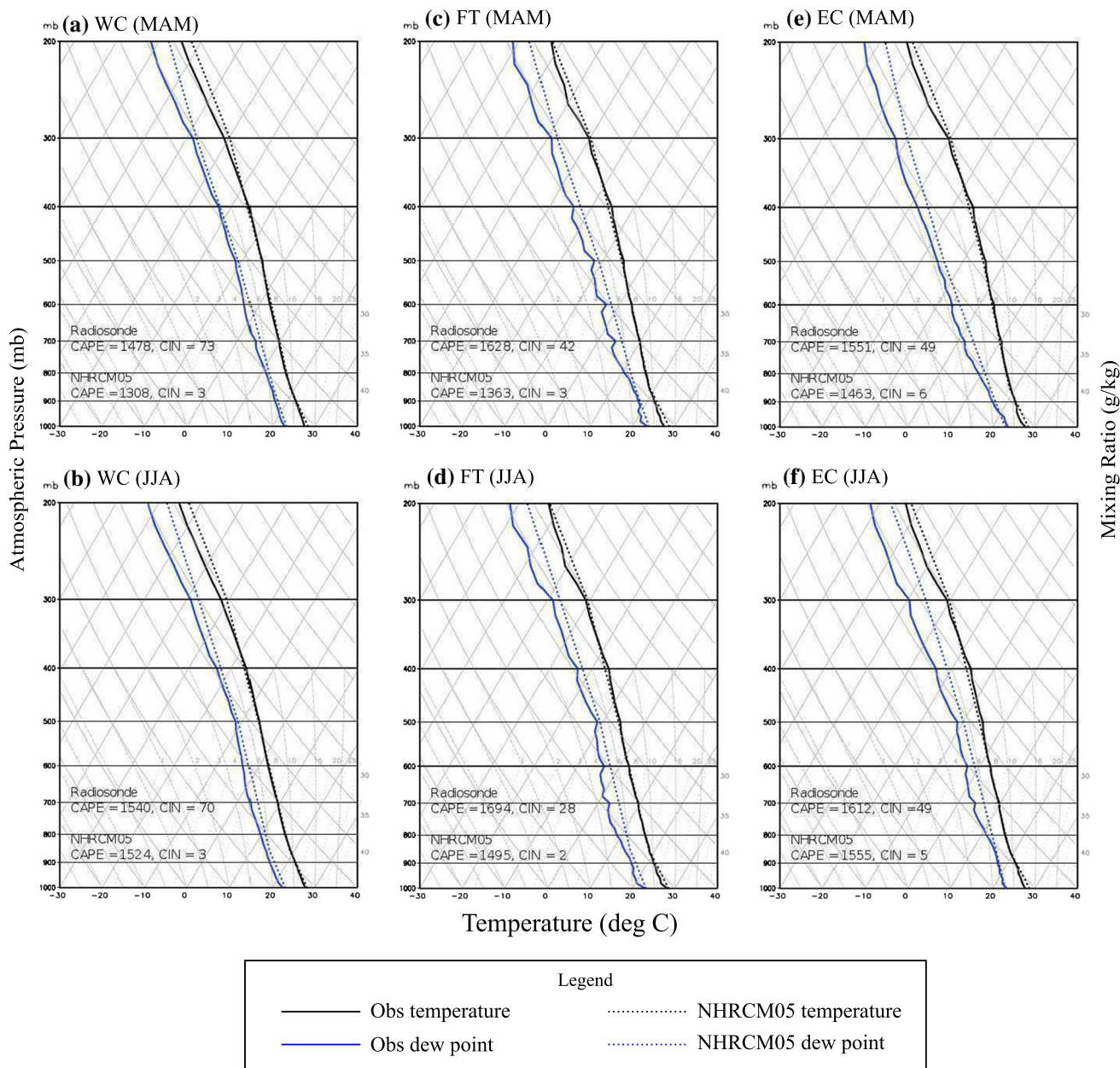
Fig. 9 Tephigrams showing seasonal mean profiles of temperature and dew point at 20:00 MST during MAM and JJA over a selected station—Sepang (**a**, **b**), Petaling Jaya (**c**, **d**), and Kota Bharu (**e**, **f**). Radiosonde temperature profiles are shown as a *solid black line* and dew point as a *solid blue line*, while NHRCM05 temperature is shown as a *dashed black line* and dew point as a *dashed blue line*. The *rows* represent different seasons, while the columns stand for different stations. The representative diurnal sub-region and season are shown at the *upper left* of each composite map. Seasonal means of CAPE and CIN from radiosondes and NHRCM05 are also shown in the tephigrams

4.4 Rainfall diurnal cycle triggering mechanisms

In general, NHRCM05 was found to perform reasonably well when simulating the diurnal rainfall and surface temperature cycle patterns. The discrepancies between observational and modelled results are similar to those found in the previous studies of RCMs elsewhere (e.g. Jeong et al. 2011; Evans and Westra 2012). Overall, there

Fig. 10 NHRCM05 simulation over Peninsular Malaysia of seasonal ▶ CAPE (**a–c**), MSE (**d–f**), and TPW (**g–i**). The *columns* represent different seasons, while the *rows* stand for the three different meteorology parameters (CAPE, MSE, and TPW)

were three main diurnal rainfall features that the model reproduced well: (1) afternoon rainfall maximum during the inter-monsoon periods over the FT sub-region; (2)
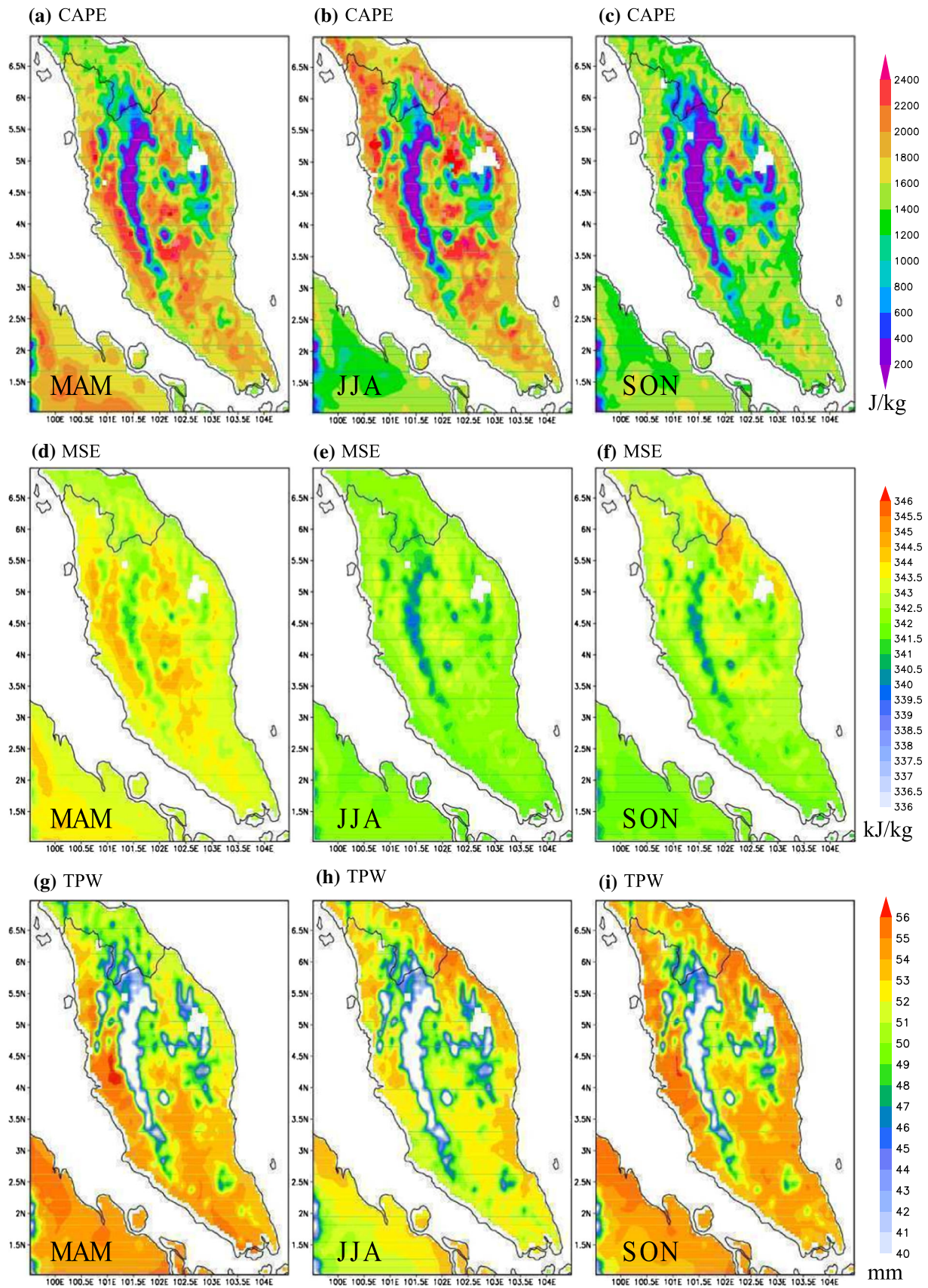
suppression of the diurnal rainfall cycle during the north-east monsoon over the EC sub-region; and (3) afternoon rainfall maximum during the northeast monsoon over the IN sub-region. Therefore, using the output of NHRCM05, the mechanisms governing these three different rainfall diurnal events can be further investigated. The output will also be analysed to understand why the model was unable to simulate the morning rainfall maximum during JJA and SON over the WC sub-region.

1. Afternoon rainfall maximum over the FT sub-region during inter-monsoon periods

In this section, the three likely factors contributing to the occurrence of an afternoon rainfall maximum over the FT sub-region are investigated, namely: conditional tropospheric instability, availability of tropospheric moisture, and local topography. To examine the conditional tropospheric instability that is preferable for convective development, we calculated the seasonal mean of CAPE (Fig. 10a–c) and vertically integrated MSE from 1000 to 300 hPa (Fig. 10d–f) at 20:00 MST over Peninsular Malaysia. For availability of tropospheric moisture, we calculated the seasonal mean of total precipitable water at 20:00 MST (Fig. 10g–i). The local time of 20:00 was selected as simulated afternoon rainfall peak tended to intensify between 18:00 MST and 22:00 MST.

The CAPE and vertically integrated MSE could be a good indicator of the potential energy that promotes convective activity over Peninsular Malaysia (Srinivasan and Smith 1996; Murugavel et al. 2012, 2014). Our investigation focused on two questions: why afternoon convection activity tends to occur during the inter-monsoon periods and why it occurs over the foothills region. Figure 10a–f

illustrates the seasonal differences of CAPE and MSE values between the inter-monsoon and southwest monsoon periods. Comparing JJA to SON, the figures show that the MSE was relatively lower in JJA, although the CAPE was high. In a conditional tropospheric instability (i.e., CAPE is greater than zero), CAPE increases with the increase of temperature and/or moisture in the boundary layer, or a decrease in temperature in the upper layers (lapse rate) (Murugavel et al. 2012, 2014). On the other hand, MSE decreases with the decrease in temperature and/or moisture in the tropospheric (boundary and upper) layer (e.g., Im et al. 2008; Yang et al. 2014). The results from Fig. 10b and c and Fig. 10e and f suggest that lower MSE over the FT sub-region during JJA are likely due to the reduction in moisture availability in the tropospheric layer. This is consistent with the reduced total precipitable water (TPW) during JJA compared with SON. Therefore, this analysis indicates that the availability of tropospheric moisture plays a major role in modulating afternoon convective rainfall, whereas a decrease in atmospheric moisture availability inhibits the convective rainfall.

To investigate the role of local topography in influencing the afternoon rainfall maximum over the FT sub-region, the surface moisture fluxes and moisture convergence at a latitude of 2.6°N–4.6°N and a longitude of 100.2°E–102.6°E at 20:00 MST were calculated (Fig. 11). This selected region is where the Titiwangsa range is likely to have a prominent influence. It is worth noting that the movement of these surface moisture fluxes is dependent on the direction and the strength of sea breezes, which are also modulated by season. During inter-monsoon periods, synoptic winds are light and variable, thus permitting the sea breezes to blow perpendicular (south-westerly) to the west
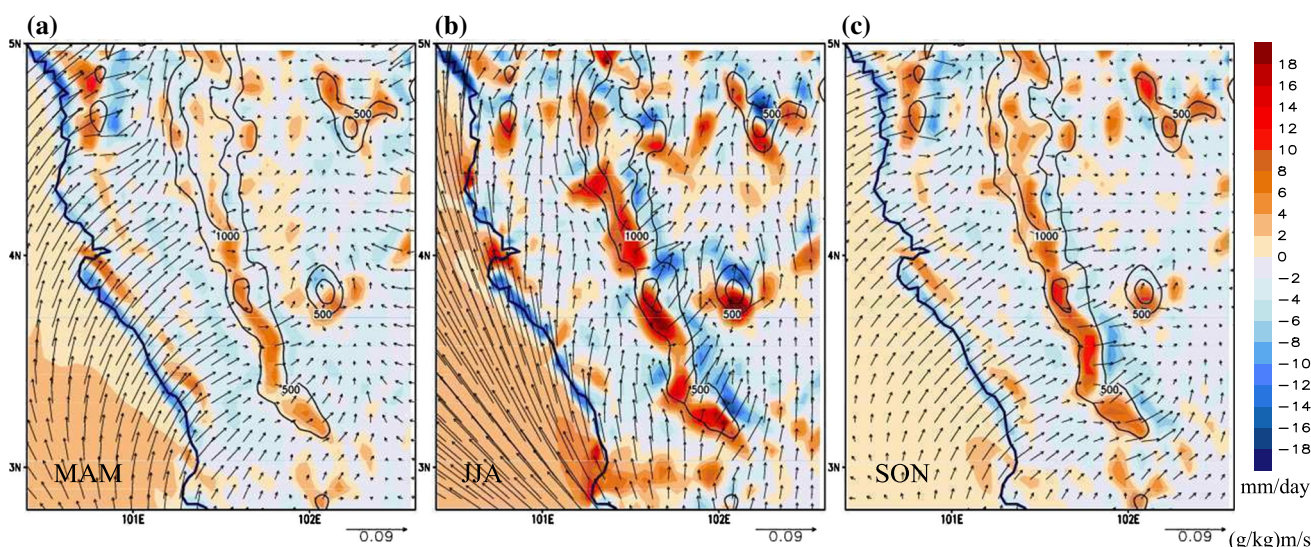

Fig. 11 Composites at 20:00 MST of NHRCM05 simulation of seasonal average moisture convergence (*shaded*, mm/day) and moisture fluxes [*vector*, (g/kg)(m/s)] during **a** MAM, **b** JJA, and **c** SON. *Blue* indicates moisture convergence, while *brown* indicates moisture divergence
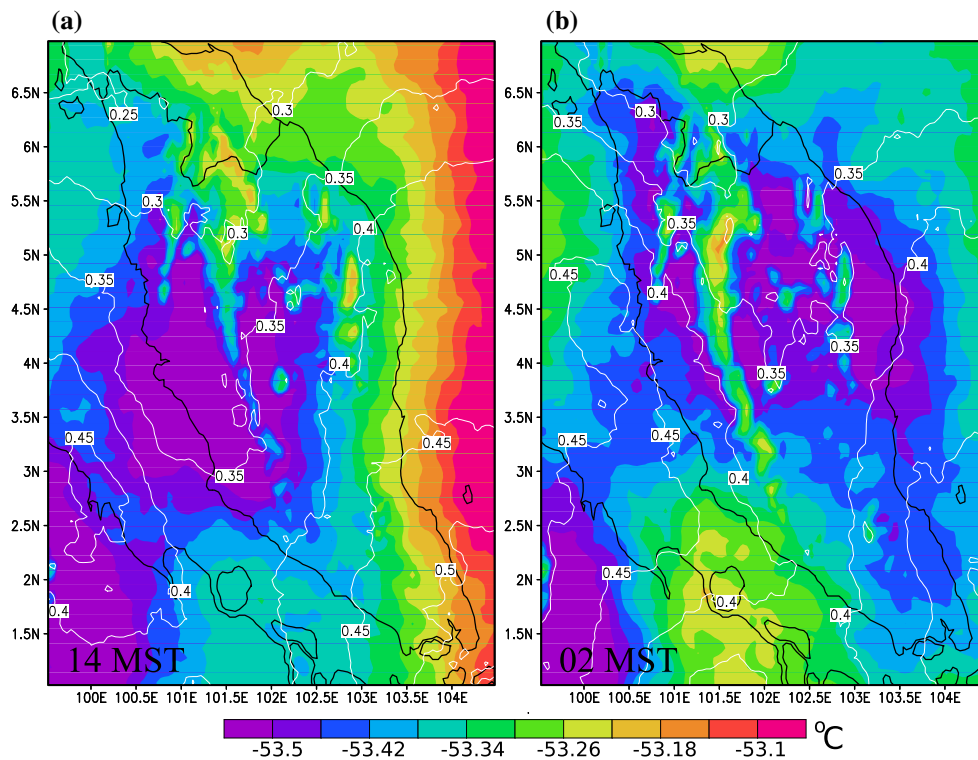
Fig. 12 Composites of NHRCM05 simulation for averaged cloud cover (*contour*) and temperature (*shaded*, °C) at **a** 14:00 MST and **b** 02:00 MST at 200 hPa during DJF. Contour interval for cloud cover is 0.05 units

coast of Peninsular Malaysia (Lim 1979). Without large-scale circulation, surface pressure gradients that develop in parallel to the shoreline in the afternoon play a major role in modulating the sea breeze direction over the region. Over the Titiwangsa mountain range, due to the terrain structure, the lower troposphere atmospheric flow was split into two types: (1) upward motion to the peak of the mountain and downward motion after the peak and (2) detouring flow around the mountain range over the lee-side of the terrain. At 20:00 MST, during the inter-monsoon periods, the surface moisture was enhanced due to the speed of convergence (flow deceleration) of the sea breeze over the mountain foothills. Similarly, the convergence of downward wind motion after the peak and the wind that detours around the range over the lee-side of mountain enhances the moisture convergence over the lee-side region (Fig. 11a, c).

During JJA, the surface synoptic wind over the west of Peninsular Malaysia was south-easterly, parallel to the coastline, and was relatively stronger than during the inter-monsoon periods (Masseran and Razali 2016). The north-eastward surface pressure gradient occurring in the afternoon interacts with the south-easterly synoptic wind, causing the sea breezes to veer in a more southerly direction (Fig. 11b). However, in the FT sub-region, the

atmospheric flow splits into two components: one parallel to the mountain range and the other going over the mountain, thus enhancing moisture divergence over this area. In contrast, the speed convergence (flow deceleration) of strong downward wind motion after the peak enhanced moisture convergence on the leeward side of the mountain (Fig. 11b).

2. Suppression of diurnal rainfall cycle during the northeast monsoon over the EC sub-region

The EC sub-region faces the southern part of the South China Sea and subsequently receives a direct impact from the strong north-easterly wind (>5 m/s) during the northeast monsoon. This north-easterly wind brings larger amounts of moisture as it travels from further north across the South China Sea (Chang et al. 2005; Chen et al. 2013). During this season, rainfall occurs throughout the entire day over the EC sub-region. Although the diurnal cycle is relatively less important than the synoptic-scale forcing in modulating the EC sub-region rainfall, the diurnal cycle still persists and plays a role in modulating rainfall. The study conducted by Lim (1979) found that in a regime of cloudy skies, the diurnal cycle is still capable of modifying the stability of the troposphere through radiational warming and cooling on the cloud tops.
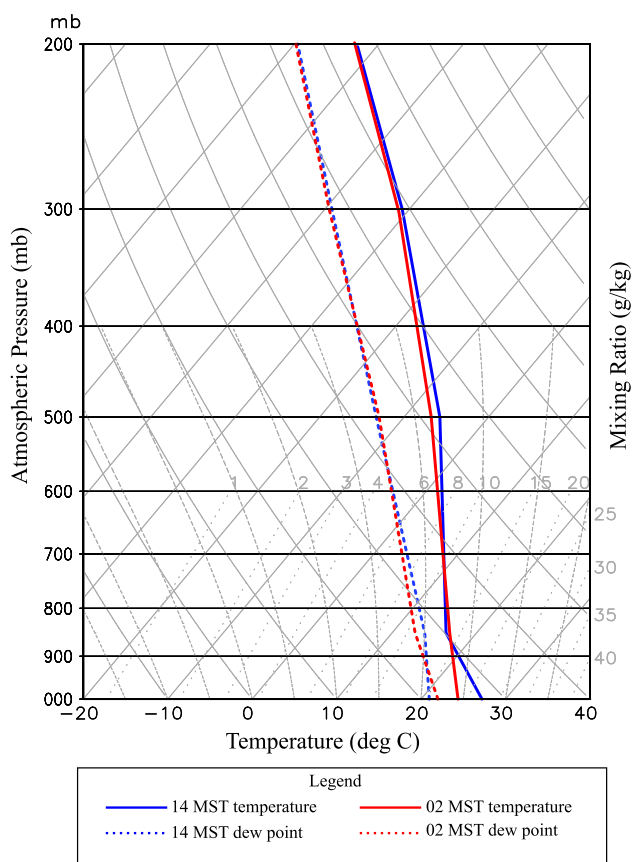
Fig. 13 NHRCM05 simulation tephigrams showing DJF mean temperature and dew point profiles at 14:00 MST and 02:00 MST, respectively. Mean profiles of temperature and dew point are averaged over single grid points corresponding to the location of Kota Bharu, Kuala Krai, Kuala Terengganu Town, Kuantan, and Mersing. Daytime temperature profiles (14:00 MST) are shown as *solid blue lines*, while the dew point profiles are *dashed blue lines*. Night-time temperature profiles (02:00 MST) are shown as *solid red lines*, and dew point profiles as *dashed red lines*

To further investigate the possible diurnal modulation of rainfall over the EC sub-region, we calculated the fractional cloud cover and temperature at the 200 hPa level at 14:00 MST and 02:00 MST as a proxy for diurnal cloud cover and temperature at the cloud top (Fig. 12). Units of fractional cloud cover in Fig. 12 are in decimal points from 0.0 to 1.0 and the contour lines are at 0.05 intervals. To visualise the changes in tropospheric stability, an average of the tropospheric profiles in the NHRCM05 grid over Kota Bharu, Kuala Krai, Kuala Terengganu Town, Kuantan, and Mersing at 14:00 MST and 02:00 MST was plotted (Fig. 13). Figure 12 shows that the EC sub-region experienced cloudy skies throughout the entire day. At 14:00 MST, the EC sub-region was dominated by fractional cloud cover of 0.40–0.50 (Fig. 12a) and the fractional cloud

cover was slightly reduced to 0.35–0.45 during the night (02:00 MST; Fig. 12b). At the same time, temperature at the cloud top over the EC sub-region was higher due to radiational warming, compared with that at 02:00 MST, when radiational cooling occurred (Fig. 12). The tropospheric profile at 14:00 MST also shows that the temperature is 1 °C lower at the cloud base (roughly at 850 hPa) and the upper tropospheric layer is warmer compared to that at 02:00 MST (Fig. 13). This indicates that the troposphere at 14:00 MST is more stable compared to at 02:00 MST over the EC sub-region. This change in atmospheric stability reduced (enhanced) the afternoon (night-time/ early morning) rainfall, resulting in the weakening of the diurnal rainfall cycle during this season (Fig. 5p).

3. **Afternoon rainfall maximum during the northeast monsoon over the IN region**

There is a remarkable difference between patterns of daily rainfall between the IN and EC sub-regions during the northeast monsoon (Fig. 5l vs. p). Despite both sub-regions experiencing rainfall throughout the day, enhanced afternoon rainfall only occurred in the IN sub-region. Figure 14 depicts the climatology of NHRCM05 rainfall amount and surface winds during the northeast monsoon at selected times. It is shown that the area of convection and occurrence of rainfall only covers the EC sub-region in the morning (Fig. 14d–f); then, in the afternoon, it expands inland to cover the IN sub-region (Fig. 14a–c). In the afternoon, the enhanced synoptic winds due to the superimposition of sea breeze and the north-easterly monsoonal wind (Fig. 14a–c) acts to expand the orographic blocking (i.e., the area experiencing flow deceleration of the incoming north-easterly monsoonal wind) toward the IN sub-region. Flow deceleration of the incoming north-easterly monsoonal wind leads to moisture convergence over the east coast of Peninsular Malaysia and often occurs in combination with local land-sea breezes (Richard 2010; Ooi et al. 2011). In contrast, in the morning, retardation of the north-easterly monsoonal wind by the land breeze reduces the area of orographic blocking and thus confines the occurrences of rainfall to the EC sub-region (Fig. 14d–f).

4. **Morning rainfall maximum during JJA and SON over the WC region**

The morning rainfall maximum during JJASON over the WC sub-region was analysed by comparing the 3-hourly rain rate derived from TRMM and NHRCM05. Overall, NHRCM05's inability to simulate the morning rainfall maximum during JJA and SON over the WC sub-region was due to its failure to resolve SSL initiation over the Malacca Straits. The 3-hourly rainfall rate derived from
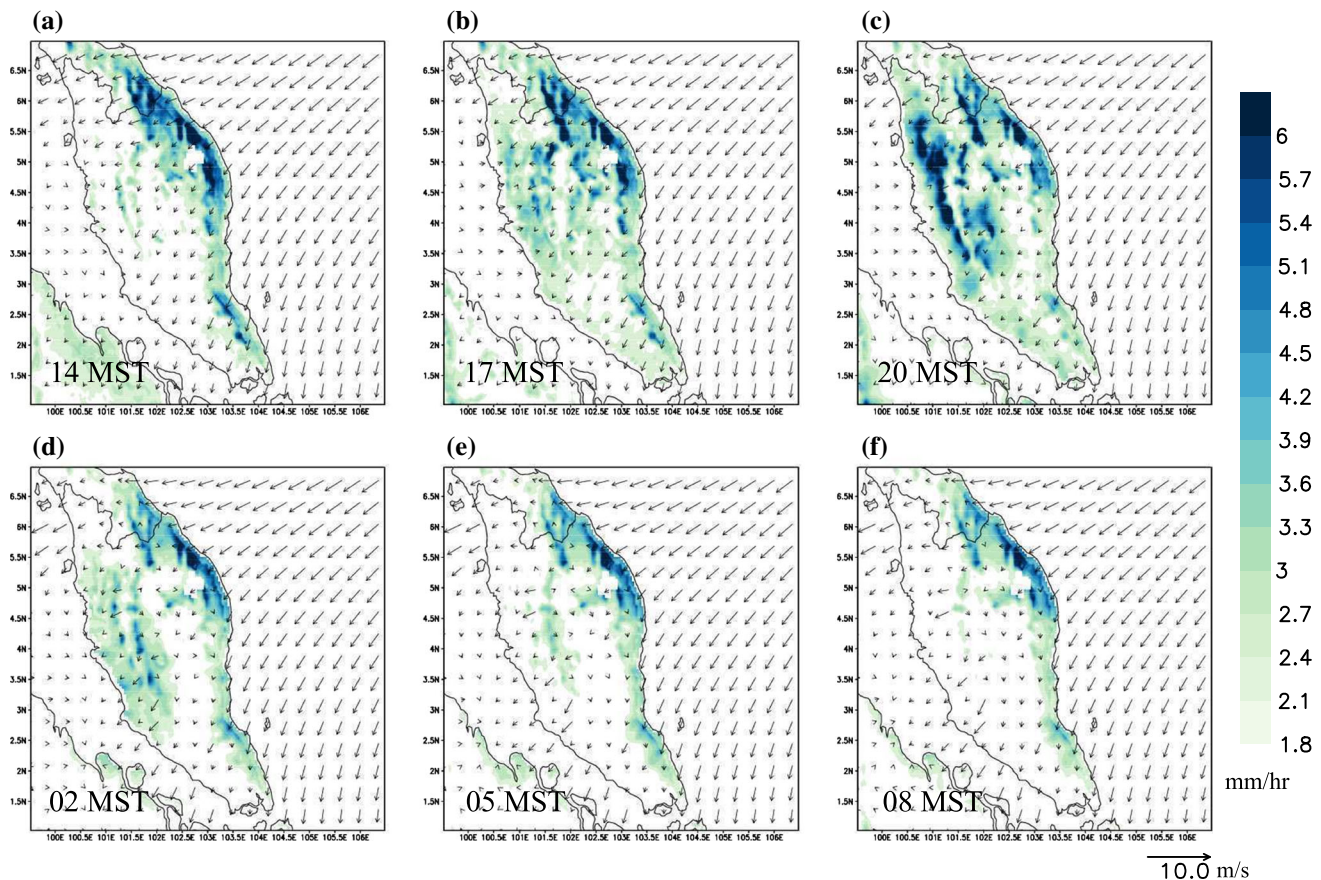
Fig. 14 Composites of spatial distributions of DJF averaged rainfall (*shaded*, mm/h) and surface wind (*vector*, m/s) at a selected hour of the NHRCM05 simulation

TRMM shows that the morning rainfall over the Malacca Straits is initiated in the early morning (02:00 MST) over the area offshore of east Sumatra (Fig. 15e). The system subsequently intensifies and decays at 11:00 MST (Fig. 15f–h). In addition to a morning convective system that was initiated and intensified over the Malacca Straits, a notable spatial rainfall gradient (0.1–0.6 mm/h) was observed over the WC sub-region, especially during 05:00 MST and 08:00 MST. This rainfall gradient was largely due to an eastward-traveling SSL, which became disorganised and dissipated rapidly once it made landfall in the coastal area (Lo and Orton 2016). The SSL tended to have different a landfall time (i.e., before dawn until late morning) and short lifespan over the land (i.e., less than an hour), and hence, the 3-hourly rainfall rate may not be able to clearly capture this eastward-traveling SSL over land (Fig. 15e–h). NHRCM05, on the other hand, was unable to resolve the initiation of morning rainfall over the Malacca Straits at 02:00 MST (Fig. 15a). Nevertheless, it did observe the rainfall over the offshore area to the west of Peninsular Malaysia at 05:00 MST, and its intensification at 08:00 MST. However, the amount of the rainfall was much lower than TRMM (Fig. 15b, c).

5 Concluding remarks

The work presented in this study explores the diurnal rainfall variability and its mechanisms across the whole of Peninsular Malaysia on a seasonal basis using a very high-resolution version of NHRCM (5 km resolution). The modelled high-resolution outputs offer a better resource for understanding the complex topography and local circulation (e.g., land–sea breezes) than the sparse observations on which the previous studies have been based (e.g. Ramage 1964; Nieuwolt 1968; Oki and Musiake 1994; Lim 1979; Richard 2010). In addition, for simplicity in understanding the diurnal rainfall mechanisms, Peninsular Malaysia was sub-divided into four distinct sub-regions, each with its own unique local processes and rainfall diurnal cycle.

The diurnal rainfall cycles over Peninsular Malaysia differ remarkably between seasons and different sub-regions. In this study, afternoon rainfall maxima over the foothills of the Titiwangsa range were shown to be significantly influenced by the availability of tropospheric moisture during the inter-monsoon periods. Consistent with the suggestion by Ramage (1964), the sea breeze was found to play a major role in transporting moisture from the

Fig. 15 Averaged 3-hourly rain rate (mm/h) over the Malacca Straits by **a** NHRCM05 and **b** TRMM during June–July–August–September–October–November (JJASON). The *rows* represent different local times in MST
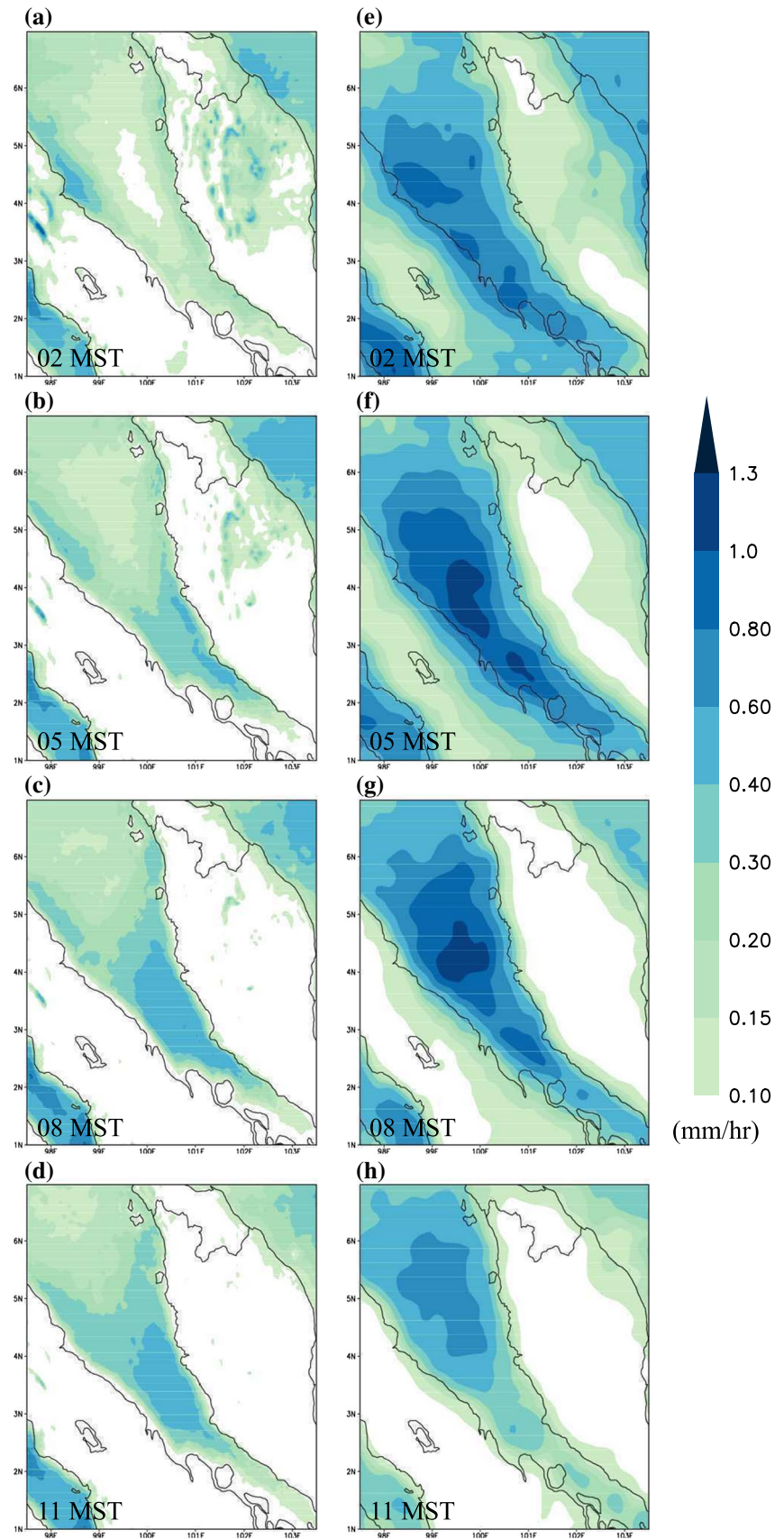
Malacca Straits to the west coast of Peninsular Malaysia. However, this study also showed that the southerly sea breeze during the southwest monsoon inhibited the formation of moisture convergence over the Titiwangsa range. This finding is inconsistent with the previous hypotheses (Ramage 1964; Nieuwolt 1968; Richard 2010), which stated that the unavailability of moisture over the west coast of Peninsular Malaysia during the southwest monsoon was due to the blocking effects of Sumatran topography.

The motion of lower tropospheric wind over the FT sub-region was divided into two motion types: (1) upward motion to the peak and downward motion after the peak and (2) detouring around the mountain range over the leeward side of the terrain (Fig. 11). These motions enhanced the orographic lifting when the wind moves upward to the mountain range peak, as well as when it converges with the detoured wind while moving downward after the peak. These motions of wind are generally consistent with Sow et al. (2011) over the FT sub-region (Klang Valley). However, the complex interactions between the sea breeze and terrain-induced gap wind over the FT sub-region could not be resolved by NHRCM05. Joseph et al. (2008) described the importance of this local circulation in modulating thunderstorm activity over the FT and WC sub-regions (Petaling Jaya and Melaka area). The inability of NHRCM05 to resolve the terrain-induced gap wind could have contributed to poor performance of the model when simulating the afternoon rainfall maximum over the FT and WC sub-regions.

In the early mornings during the northeast monsoon, the convection mainly occurred over the EC sub-region due to the retardation of the north-easterly wind by the land breeze and orographic blocking. During the afternoon, the superimposition of the sea breeze on the north-easterly monsoonal wind strengthened the north-easterly wind, thus causing the zone of convection to expand further inland. This generally explains the morning and afternoon rainfall maximum over the WC and IN regions, respectively. In addition, during this season, the diurnal rainfall cycle is relatively suppressed over the EC sub-region. The modelling result shows that the atmospheric stability increases during the daytime, while it decreases during the night-time. This finding is consistent with that of Lim (1979) over the northeast of Peninsular Malaysia, where the diurnal rainfall was suppressed.

During the southwest monsoon and SON, NHRCM05 was unable to capture the morning rainfall maximum. This failure was caused by the inability of NHRCM05 to resolve SSL initiation over the Malacca Straits, which might be due to the use of insufficient resolution. Lane et al. (2001) and Bhatt et al. (2016) argued that a model resolution of at least 4 km (convection-permitting scale) is required for this

SSL initiation. Furthermore, failure to resolve the east-ward-traveling SSL may also be a contributing factor. Pritchard et al. (2011) and Gianotti (2013) showed that the eastward-traveling SSL could not be captured in simulations with the conventional CPS, as the schemes lacked the proper representation of cold outflows. The absence of cold outflows from convective downdrafts appears to be critical for the eastward-traveling SSL, as the cold outflows allow the simulation of self-generating convection in the SSL system. Therefore, simulation with a model at a convection-permitting resolution may be needed for better simulation of the southwest monsoon and SON morning rainfall maximum.

References

Argüeso D, Di Luca A, Evans JP (2016) Precipitation over urban areas in the western Maritime Continent using a convection-permitting model. Clim Dyn 47:1143–1159. doi:10.1007/s00382-015-2893-6

Bhatt BC, Sobolowski S, Higuchi A (2016) Simulation of diurnal rainfall variability over the Maritime Continent with a high-resolution regional climate model. J Meteorol Soc Japan Ser II 94A:89–103. doi:10.2151/jmsj.2015-052

Birch CE, Webster S, Peatman SC, Parker DJ, Matthews AJ, Li Y, Hassim ME (2016) Scale interactions between the MJO and the western Maritime Continent. J Clim 29:2471–2492. doi:10.1175/JCLI-D-15-0557.1

Brockhaus P, Lüthi D, Schär C (2008) Aspects of the diurnal cycle in a regional climate model. Meteorol Zeitschrift 17:433–443. doi:10.1127/0941-2948/2008/0316

Ceglar A, Toreti A, Balsamo G, Kobayashi S (2017) Precipitation over monsoon Asia: a comparison of reanalyses and observations. J Clim 30:465–476. doi:10.1175/JCLI-D-16-0227.1

Chang C-P, Harr PA, Chen H-J (2005) Synoptic disturbances over the equatorial South China Sea and western Maritime Continent during boreal winter. Mon Weather Rev 133:489–503. doi:10.1175/MWR-2868.1

Chen T-C, Tsay J-D, Yen M-C, Matsumoto J (2013) The winter rainfall of Malaysia. J Clim 26:936–958. doi:10.1175/JCLI-D-12-00174.1

Choi IJ, Jin EK, Han JY et al (2015) Sensitivity of diurnal variation in simulated precipitation during East Asian summer monsoon to cumulus parameterization schemes. J Geophys Res Atmos 120:11971–11987. doi:10.1002/2015JD023810

Chung J, Juneng L, Tangang F, Jamaluddin AF (2017) Performance of BATS and CLM land surface schemes in RegCM4 in simulating precipitation over the CORDEX Southeast Asia Domain. Int J Climatol. doi:10.1002/joc.5211

Cruz FT, Sasaki H (2017) Simulation of present climate over Southeast Asia using the non-hydrostatic regional climate model. Sola 13:13–18. doi:10.2151/sola.2017-003

Cruz FT, Sasaki H, Narisma GT (2016) Assessing the sensitivity of the non-hydrostatic regional climate model to boundary conditions and convective schemes over the Philippines. J Meteorol Soc Japan 94A:165–179. doi:10.2151/jmsj.2015-059

Cruz FT, Narisma GT, Dado JM, Singhruck P, Tangang FT, Linarka UA, Wati T, Juneng L, Phan-Van T, Ngo-Duc T, Santisirisomboon J, Gunawan D, Aldrian E (2017) Sensitivity of temperature to physical parameterization schemes of RegCM4 over the CORDEX-Southeast Asia Region. Int J Climatol. doi:10.1002/joc.5151

Evans JP, Westra S (2012) Investigating the mechanisms of diurnal rainfall variability using a regional climate model. J Clim 25:7232–7247. doi:10.1175/JCLI-D-11-00616.1

Fersch B, Kunstmann H (2013) Atmospheric and terrestrial water budgets: sensitivity and performance of configurations and global driving data for long-term continental scale WRF simulations. Clim Dyn 42:2367–2396. doi:10.1007/s00382-013-1915-5

Francisco RV, Argete J, Giorgi F et al (2006) Regional model simulation of summer rainfall over the Philippines: effect of choice of driving fields and ocean flux schemes. Theor Appl Climatol 86:215–227. doi:10.1007/s00704-005-0216-2

Fujita M, Kimura F, Yoshizaki M (2010) Morning precipitation peak over the Strait of Malacca under a calm condition. Mon Weather Rev 138:1474–1486. doi:10.1175/2009MWR3068.1

Gianotti RL (2013) Convective cloud and rainfall processes over the maritime continent: simulation and analysis of the diurnal cycle. Dissertation, Massachusetts Institute of Technology

Gianotti RL, Zhang D, Eltahir EAB (2012) Assessment of the regional climate model version 3 over the Maritime Continent using different cumulus parameterization and land surface schemes. J Clim 25:638–656. doi:10.1175/JCLI-D-11-00025.1

Giorgi F, Bi X, Pal J (2004a) Mean, interannual variability and trends in a regional climate change experiment over Europe. II: climate change scenarios (2071–2100). Clim Dyn 23:839–858. doi:10.1007/s00382-004-0467-0

Giorgi F, Bi X, Pal JS (2004b) Mean, interannual variability and trends in a regional climate change experiment over Europe. I. present-day climate (1961–1990). Clim Dyn 22:733–756. doi:10.1007/s00382-004-0409-x

Hassim MEE, Lane TP, Grabowski WW (2016) The diurnal cycle of rainfall over New Guinea in convection-permitting WRF simulations. Atmos Chem Phys 16:161–175. doi:10.5194/acp-16-161-2016

Hirai M, Ohizumi M (2004) Development of a new land-surface Model for JMA-GSM. In: 20th Conference on Weather Analysis and Forecasting/16th Conference on Numerical Weather Prediction. Available at https://ams.confex.com/ams/84Annual/techprogram/paper_68652.htm. pp 9–10

Huffman GJ, Adler RF, Bolvin DT, Gu G, Nelkin EJ, Bowman KP, Stocker EF, Wolff DB (2007) The TRMM multi-satellite precipitation analysis: quasi-global, multi-year, combined-sensor precipitation estimates at fine scale. J Hydrometeorol 8:33–55

Im E-S, Ahn J-B, Remedio AR, Kwon W-T (2008) Sensitivity of the regional climate of East/Southeast Asia to convective parameterizations in the RegCM3 modelling system. Part 1: focus on the Korean peninsula. Int J Climatol 28:1861–1877. doi:10.1002/joc.1664

Iorio JP, Duffy PB, Govindasamy B et al (2004) Effects of model resolution and subgrid-scale physics on the simulation of precipitation in the continental United States. Clim Dyn 23:243–258. doi:10.1007/s00382-004-0440-y

Ishii M, Shouji A, Sugimoto S, Matsumoto T (2005) Objective analyses of sea-surface temperature and marine meteorological variables for the 20th century using ICOADS and the Kobe Collection. Int J Climatol 25:865–879. doi:10.1002/joc.1169

Jeong J-H, Walther A, Nikulin G et al (2011) Diurnal cycle of precipitation amount and frequency in Sweden: observation versus model simulation. Tellus A 63:664–674. doi:10.1111/j.1600-0870.2011.00517.x

Joseph B, Bhatt BC, Koh TY, Chen S (2008) Sea breeze simulation over the Malay Peninsula in an intermonsoon period. J Geophys Res 113:D20122. doi:10.1029/2008JD010319

Juneng L, Tangang F, Chung J et al (2016) Sensitivity of Southeast Asia rainfall simulations to cumulus and air-sea flux parameterizations in RegCM4. Clim Res 69:59–77. doi:10.3354/cr01386

Kain JS (2004) The Kain-Fritsch convective parameterization: an update. J Appl Meteorol 43:170–181

Kida H, Koide T, Sasaki H, Chiba M (1991) A new approach for coupling a limited area model to a GCM for regional climate simulations. J Meteorol Soc Japan 69:723–728

Kieu-Thi X, Vu-Thanh H, Nguyen-Minh T et al (2016) Rainfall and tropical cyclone activity over Vietnam simulated and projected by the non-hydrostatic regional climate model; NHRCM. J Meteorol Soc Japan Ser II 94A:135–150. doi:10.2151/jmsj.2015-057

Kikuchi K, Wang B (2008) Diurnal precipitation regimes in the global tropics. J Clim 21:2680–2696. doi:10.1175/2007JCLI2051.1

Kobayashi C, Iwasaki T (2016) Brewer-Dobson circulation diagnosed from JRA-55. J Geophys Res Atmos 121:1493–1510. doi:10.1002/2015JD023476

Kobayashi S, Ota Y, Harada Y et al (2015) The JRA-55 reanalysis: general specifications and basic characteristics. J Meteorol Soc Japan Ser II 93:5–48. doi:10.2151/jmsj.2015-001

Koo M-S, Hong S-Y (2010) Diurnal variations of simulated precipitation over East Asia in two regional climate models. J Geophys Res 115:1–17. doi:10.1029/2009JD012574

Kwan MS, Tangang FT, Juneng L (2014) Present-day regional climate simulation over Malaysia and western Maritime Continent region using PRECIS forced with ERA40 reanalysis. Theor Appl Climatol 115:1–14. doi:10.1007/s00704-013-0873-5

Lane T, Reeder M, Clark T (2001) Numerical modeling of gravity wave generation by deep tropical convection. J Atmos Sci 58:1249–1274. doi:10.1175/1520-0469(2001)058

Loh JL, Tangang F, Juneng L et al (2016) Projected rainfall and temperature changes over Malaysia at the end of the 21st century based on PRECIS modelling system. Asia–Pacific J Atmos Sci 52:191–208. doi:10.1007/s13143-016-0019-7

Lim JT (1979) Characteristics of the winter monsoon over the Malaysian region. Dissertation, University of Hawaii

Lo JCF, Orton T (2016) The general features of tropical Sumatra squalls. Weather 71:175–178. doi:10.1002/wea.2748

Mapes BE (2000) Convective inhibition, subgrid-scale triggering energy, and stratiform instability in a toy tropical wave model. J Atmos Sci 57:1515–1535. doi:10.1175/1520-0469(2000)057

Masseran N, Razali AM (2016) Modeling the wind direction behaviors during the monsoon seasons in Peninsular Malaysia. Renew Sustain Energy Rev 56:1419–1430. doi:10.1016/j.rser.2015.11.040

Mohd MSF, Juneng L, Tangang F et al (2015) Simulation of upper Kuantan River basin streamflow using SWAT model. AIP Conf Proc 1678:020021. doi:10.1063/1.4931206

Mori S, Jun-Ichi H, Tauhid YI et al (2004) Diurnal land–sea rainfall peak migration over Sumatera Island, Indonesian Maritime Continent, observed by TRMM satellite and intensive rawinsonde soundings. Mon Weather Rev 132:2021–2039

Murugavel P, Pawar SD, Gopalakrishnan V (2012) Trends of convective available potential energy over the Indian region and its effect on rainfall. Int J Climatol 32:1362–1372. doi:10.1002/joc.2359

Murugavel P, Pawar SD, Gopalakrishan V (2014) Climatology of lightning over Indian region and its relationship with convective

available potential energy. Int J Climatol 34:3179–3187. doi:10.1002/joc.3901

Myoung B, Nielsen-Gammon JW (2010) Sensitivity of monthly convective precipitation to environmental conditions. J Clim 23:166–188. doi:10.1175/2009JCLI2792.1

Nakano M, Kato T, Hayashi S et al (2012) Development of a 5-km-mesh cloud-system-resolving regional climate model at the Meteorological Research Institute. J Meteorol Soc Japan 90A:339–350. doi:10.2151/jmsj.2012-A19

Ngo-Duc T, Tangang FT, Santisirisomboon J et al (2016) Performance evaluation of RegCM4 in simulating extreme rainfall and temperature indices over the CORDEX-Southeast Asia region. Int J Climatol 37:1634–1647. doi:10.1002/joc.4803

Nieuwolt S (1968) Diurnal rainfall variation in Malaya1. Ann Assoc Am Geogr 58:313–326

Oki T, Musiake K (1994) Seasonal change of the diurnal cycle of precipitation over Japan and Malaysia. J Appl Meteorol 33:1445–1463

Ooi SH, Samah AA, Braesicke P (2011) A case study of the Borneo Vortex genesis and its interactions with the global circulation. J Geophys Res Atmos 116:D21116. doi:10.1029/2011JD015991

Pritchard MS, Moncrieff MW, Somerville RCJ (2011) Orogenic propagating precipitation systems over the United States in a Global Climate Model with embedded explicit convection. J Atmos Sci 68:1821–1840. doi:10.1175/2011JAS3699.1

Raghavan SV, Vu MT, Liong SY (2015) Regional climate simulations over Vietnam using the WRF model. Theor Appl Climatol 126:161–182. doi:10.1007/s00704-015-1557-0

Räisänen J, Hansson U, Ullerstig A et al (2004) European climate in the late twenty-first century: regional simulations with two driving global models and two forcing scenarios. Clim Dyn 22:13–31. doi:10.1007/s00382-003-0365-x

Raktham C, Bruyère C, Kreasuwun J, Done J, Thongbai C, Promnopas W (2015) Simulation sensitivities of the major weather regimes of the Southeast Asia region. Clim Dyn 44:1403–1417

Ramage CS (1964) Diurnal variation of summer rainfall of Malaya. J Trop Geogr 19:62–68

Ramella Pralungo L, Haimberger L, Stickler A (2014) A global radiosonde and tracked balloon archive on 16 pressure levels (GRASP) back to 1905: Part 1: merging and interpolation to 00:00 and 12:00 GMT. Earth Syst Sci Data 6:185–200. doi:10.5194/essd-6-185-2014

Ratna S, Ratnam J, Behera S et al (2017) Validation of the WRF regional climate model over the subregions of Southeast Asia: climatology and interannual variability. Clim Res 71:263–280. doi:10.3354/cr01445

Richard SS (2010). The diurnal variations of rainfall and winds over Malaysia. Dissertation, University of Hawaii at Manoa

Saito K, Fujita T, Yamada Y et al (2006) The operational JMA nonhydrostatic mesoscale model. Mon Weather Rev 134:1266–1298. doi:10.1175/MWR3120.1

Saito K, Ishida J, Aranami K et al (2007) Nonhydrostatic atmospheric models and operational development at JMA. J Meteorol Soc Japan 85B:271–304. doi:10.2151/jmsj.85B.271

Sasaki H, Sato Y, Adachi K, Kida H (2000) Performance and evaluation of the MRI regional climate model with the spectral boundary coupling method. J Meteorol Soc Japan 78:477–489

Sasaki H, Kurihara K, Takayabu I, Uchiyama T (2008) Preliminary experiments of reproducing the present climate using the non-hydrostatic regional climate model. Sola 4:25–28. doi:10.2151/sola.2008-007

Siew JH, Tangang FT, Juneng L (2014) Evaluation of CMIP5 coupled atmosphere-ocean general circulation models and projection of the Southeast Asian winter monsoon in the 21st century. Int J Climatol 34:2872–2884. doi:10.1002/joc.3880

Sow KS, Juneng L, Tangang FT et al (2011) Numerical simulation of a severe late afternoon thunderstorm over Peninsular Malaysia. Atmos Res 99:248–262

Srinivasan J, Smith GL (1996) The role of heat fluxes and moist static energy in Tropical Convergence Zones. Mon Weather Rev 124:2089–2099. doi:10.1175/1520-0493(1996)124

Sun Y, Solomon S, Dai A, Portmann RW (2006) How often does it rain? J Clim 19:916–934. doi:10.1175/JCLI3672.1

Sun B, Reale A, Seidel DJ, Hunt DC (2010) Comparing radiosonde and COSMIC atmospheric profile data to quantify differences among radiosonde types and the effects of imperfect collocation on comparison statistics. J Geophys Res Atmos 115:1–16. doi:10.1029/2010JD014457

Tangang FT, Juneng L, Salimun E et al (2008) On the roles of the northeast cold surge, the Borneo Vortex, the Madden-Julian Oscillation, and the Indian Ocean Dipole during the extreme 2006/2007 flood in southern Peninsular Malaysia. Geophys Res Lett 35:1–6. doi:10.1029/2008GL033429

Tangang FT, Juneng L, Salimun E et al (2012) Climate change and variability over Malaysia: gaps in science and research information. Sains Malaysiana 41:1355–1366

Van Phan T, Van Nguyen H, Trinh Tuan L et al (2014) Seasonal prediction of surface air temperature across Vietnam using the Regional Climate Model Version 4.2 (RegCM4.2). Adv Meteorol 2014:1–13. doi:10.1155/2014/245104

Wang Y, Zhou L, Hamilton K (2007) Effect of convective entrainment/detrainment on the simulation of the tropical precipitation diurnal cycle. Mon Weather Rev 135:567–585. doi:10.1175/MWR3308.1

Wong CL, Venneker R, Jamil ABM, Uhlenbrook S (2011) Development of a gridded daily hydrometeorological data set for Peninsular Malaysia. Hydrol Process 25:1009–1020. doi:10.1002/hyp.7654

Wong C, Liew J, Yusop Z et al (2016) Rainfall characteristics and regionalization in Peninsular Malaysia based on a high resolution gridded data set. Water 8:500. doi:10.3390/w8110500

Yang B, Zhang Y, Qian Y et al (2014) Calibration of a convective parameterization scheme in the WRF model and its impact on the simulation of East Asian summer monsoon precipitation. Clim Dyn 44:1661–1684. doi:10.1007/s00382-014-2118-4

Yasunaga K, Sasaki H, Wakazuki Y et al (2005) Performance of long-term integrations of the Japan meteorological agency nonhydrostatic model using the spectral boundary coupling method. Wea Forecast 20:1061–1072. doi:10.1175/WAF894.1

Zhou T, Yu R, Chen H et al (2008) Summer precipitation frequency, intensity, and diurnal cycle over China: a comparison of satellite data with rain gauge observations. J Clim 21:3997–4010. doi:10.1175/2008JCLI2028.1